TAPHONOMY, GEOLOGICAL AGE, AND PALEOBIOGEOGRAPHY OF *LOTOSAURUS ADENTUS* (ARCHOSAURIA: POPOSAUROIDEA) FROM THE MIDDLE-UPPER TRIASSIC BADONG FORMATION, HUNAN, CHINA

Author(s): CEDRIC J. HAGEN, ERIC M. ROBERTS, CORWIN SULLIVAN, JUN LIU, YANYIN WANG, PRINCE C. OWUSU AGYEMANG, and XING XU
Source: PALAIOS, 33(3):106-124.
Published By: Society for Sedimentary Geology
URL: http://www.bioone.org/doi/full/10.2110/palo.2017.084

PALAIOS
Emphasizing the impact of life on Earth's history

PALAIOS, 2018, v. 33, 106–124
Research Article
DOI: http://dx.doi.org/10.2110/palo.2017.084

TAPHONOMY, GEOLOGICAL AGE, AND PALEOBIOGEOGRAPHY OF *LOTOSAURUS ADENTUS* (ARCHOSAURIA: POPOSAUROIDEA) FROM THE MIDDLE-UPPER TRIASSIC BADONG FORMATION, HUNAN, CHINA

CEDRIC J. HAGEN,[1,2] ERIC M. ROBERTS,[2] CORWIN SULLIVAN,[3,4] JUN LIU,[5,6] YANYIN WANG,[3] PRINCE C. OWUSU AGYEMANG,[2] AND XING XU[5]

[1]*College of Earth, Ocean and Atmospheric Sciences, Oregon State University, Corvallis, Oregon, 97333, USA*
[2]*Geosciences, College of Science and Engineering, James Cook University, Townsville, QLD 4811, Australia*
[3]*Department of Biological Sciences, University of Alberta, Edmonton, AB T6G 2E9, Canada*
[4]*Philip J. Currie Dinosaur Museum, Wembley, AB T0H 3S0, Canada*
[5]*Key Laboratory of Vertebrate Evolution and Human Origins, Institute of Vertebrate Paleontology and Paleoanthropology, Beijing 100044, China*
[6]*University of Chinese Academy of Sciences, Beijing 100049, China*
email: eric.roberts@jcu.edu.au

ABSTRACT: ***Lotosaurus adentus* is an unusual sail-backed, edentulous poposauroid pseudosuchian primarily known from a single, nearly monospecific bonebed discovered and excavated in the 1970s in the Middle-Upper Triassic Badong Formation of Sangzhi County, Hunan Province, South China. Renewed interest in this unique taxon prompted exposure of an additional 90 m^2 of the bonebed. Almost 1000 new *L. adentus* bones, 28% of which were articulated, were discovered during this excavation. The bones lack evidence of tooth marks, trample marks, or insect modification, and display minimal weathering. The site is reinterpreted as a pedogenically modified floodplain pond (and overlying fluvial channel) within a warm, semi-arid sub-tropical region (paleolatitude $\sim 34^{\circ}$N), contrasting with previous interpretations of the locality as a tidal flat deposit. The occurrence of mudcracks, conchostrachan fossils, and vertic paleosol development with calcium carbonate accumulations in both overlying and underlying facies indicates periodic aridity and ephemeral conditions. The bonebed is characterized by partial disarticulation and minor transport, and is confined to a thin, $<$ 30 cm-thick interval. Considered together, these features are most consistent with a mass mortality event, possibly drought related considering the sedimentological context, followed by minor transport during a rapid burial event.**

U-Pb detrital zircon geochronology and Lu-Hf isotope analysis were utilized to reassess the provenance and age of the deposit, and suggest that *L. adentus* was likely Ladinian or possibly even Carnian in age, rather than Anisian as previously reported. Paleocurrent data, detrital zircon age spectra, and Lu-Hf isotopes indicate that fluvial sediments were partially derived from sources in the North China craton and Qinling-Dabieshan tectonic belt, implying that faunal interchange between the North and South China blocks was possible by this time.

INTRODUCTION

Poposauroidea is a morphologically disparate clade of pseudosuchian (e.g., crocodylian-line) archosaurs with a wide Pangean distribution and a documented stratigraphic range encompassing most of the Triassic, extending from the upper Olenekian to the upper Norian (Butler et al. 2011; Nesbitt et al. 2013). A particularly distinctive member of this group is the Chinese species *Lotosaurus adentus*, which exhibits the unusual combination of an edentulous skull, a dorsal "sail" comprising elongate neural spines, and limb proportions indicative of quadrupedality (Zhang 1975; Parrish 1993; Gower 2000; Nesbitt 2011). Although the affinities of *L. adentus* were unclear for decades, recent phylogenetic analyses (Brusatte et al. 2010; Nesbitt 2011; Butler et al. 2011) have unanimously recovered *L. adentus* as a poposauroid. *Lotosaurus adentus* is primarily known from a single bonebed in Sangzhi County, Hunan Province, southern China (Fig. 1), which was discovered in 1970 and first described by Zhang (1975). The bonebed, which we term the "*Lotosaurus* Quarry", is traditionally dated to the Middle Triassic (Anisian), and yielded hundreds of individual bones and a number of partial skeletons during excavations in the 1970s and 1980s. Small numbers of disarticulated bones possibly attributable to *L. adentus* have also been reported from Maopingchang Township, Yuanan County, Hubei Province (Liu and Wang 2005).

The tectonic assembly of southern China occurred at least partially during the Middle Triassic, and was characterized by closing of the Tethys Sea and collision between the South and North China Cratons (SCC, NCC) along a boundary approximating the course of the present day Yangtze River, north of the *Lotosaurus* Quarry (e.g., the quarry is on the northern margin of the SCC; Metcalfe 2013). Most recent paleogeographic and paleobiogeographic reconstructions depict the NCC and the SCC as isolated islands during the Late Permian and Early Triassic (e.g., Metcalfe 2013; Matthews et al. 2016). The precise timing of collision, and specifically the timing of terrestrial connectivity and faunal interchange, remains uncertain within the Early to Middle Triassic but has interesting implications for the origins of *L. adentus* and other Chinese vertebrates of the same age. For instance, was *L. adentus* originally endemic to the SCC or to the NCC? If the latter, individuals presumably migrated from the NCC to the SCC once a connection was established. If collision between the NCC and SCC predated the *Lotosaurus* Quarry, then *L. adentus* could

Published Online: March 2018
 0883-1351/18/033-106/$03.00

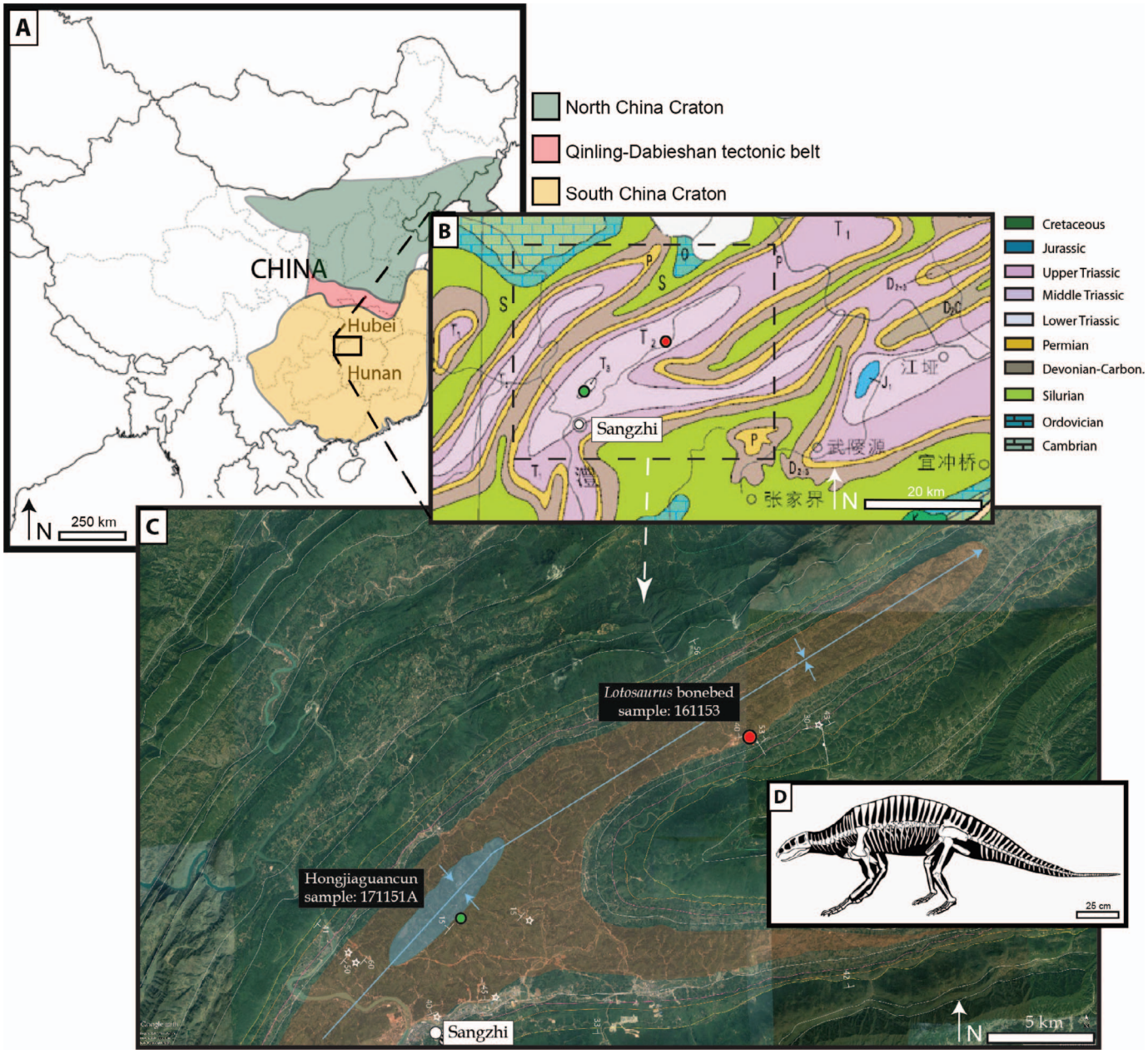

FIG. 1.—Location of the *Lotosaurus* Quarry in northern Hunan, China. **A**) Overview map of China with location of study area indicated by black box. **B**) Geologic map of SW Hubei and NW Hunan provinces with locations of study sites shown by colored circles (dashed black box shows location of C). **C**) Google Earth image showing the vicinity of the *Lotosaurus* Quarry and other study sites, including detrital zircon sample localities. **D**) Skeleton of *L. adentus*.

be endemic to either craton, whereas if the collision occurred after formation of the bonebed then *L. adentus* must have originated on the SCC. Most previous workers have interpreted the Badong Formation as primarily lagoonal, tidal flat, or storm tidal, albeit possibly with some indication of fluvial influence (Zhang 1975; Meng et al. 1995). Such conclusions suggest that the Tethys Sea still represented a barrier to faunal interchange between the NCC and SCC during the Middle Triassic, but more detailed investigation of the *L. adentus*-bearing interval is required to test this inference.

Little work has been conducted on *L. adentus* since the original description by Zhang (1975), and neither the biogeographic origins of this taxon nor the taphonomy of the *Lotosaurus* Quarry have been investigated in detail. In 2012, we contracted with local museum and community members to renew excavations at the *Lotosaurus* Quarry, uncovering approximately 1000 new *L. adentus* bones, some of which remained in articulation, across a $\sim$ 90 m^2 steeply dipping (40°NW) bedding surface. Almost all these bones were left in place on the exposed rock surface. We returned to the locality in 2015 to study its taphonomy, in addition to the sedimentology and stratigraphy of the part of the Badong Formation containing the *Lotosaurus* Quarry.

Here we present a detailed analysis of the bonebed and a geologic investigation of the Badong Formation in northwestern Hunan Province. Our study aims to better constrain the taphonomic and paleoenvironmental factors that facilitated the formation of the *Lotosaurus* Quarry, providing essential context for study of the evolutionary history and paleobiology of the unusual poposauroid *L. adentus*. We also used U-Pb detrital zircon

geochronology to more precisely estimate the age of the fossil locality and improve regional correlations with other parts of the Badong Formation, in order to refine recent paleogeographic reconstructions and assess competing hypotheses regarding the paleobiogeographic origin of *L. adentus*.

GEOLOGIC BACKGROUND

The *Lotosaurus* Quarry is located in northwestern Hunan Province, ~ 20 km northeast of the urban seat of Sangzhi County in the prefecture-level city of Zhangjiajie. The site was first discovered during regional geologic mapping of the Sangzhi area in 1970 (Zhang 1975). It is located within a steeply dipping succession of Middle to Upper Triassic redbeds referred to as the Badong Formation on the southern limb of a large syncline, near the township of Furongqiao (29°23′33.97"N, 110°9′49.52"E) (Fig. 1).

The region is characterized geologically by extensive upper Paleozoic–lower Mesozoic carbonate and siliciclastic strata that were deposited as part of the shallow Yangtze Platform sequence on the northern margin of the SCC (Enos et al. 2006). By the late Permian, closure of the Tethys Sea was underway as the SCC moved rapidly northwards towards the NCC. Continental collision between the two blocks occurred sometime during the Middle to Late Triassic, with the precise timing of this event still widely debated (e.g., Matthews et al. 2016). This collisional event produced the Qinling-Dabieshan (QD) tectonic belt along the suture between the NCC and the SCC (Fig. 1; Guo et al. 2012). Thick flysch sequences indicate that a shift in deposition from predominantly carbonate to predominantly siliciclastic occurred on the Yangtze Platform, as continental facies prograded westward in association with the progressing collision (Enos et al. 2006). The collision resulted in the uplift, folding and exposure of extensive upper Paleozoic–Upper Triassic Yangtze Platform sequences throughout much of Hubei, Hunan, and Guizhou provinces, as well as the city of Chongqing, in what is now referred to as the Jiangnan fold and thrust belt (Liu et al. 2005).

Badong Formation Stratigraphy

The Badong Formation, which hosts the *Lotosaurus* Quarry, is subdivided into five discrete members (Huang and Opdyke 1996). Zhang (1975) interpreted the site as part of the lower to middle portion of the Badong Formation (member 2), which is widely distributed across parts of Hubei, Hunan, Chongqing, and Guizhou. Member 1 is ~ 80 m thick in the type section, located near Badong in southern Hubei, and defined as a series of gray, calcareous shales with thinly bedded limestones and dolomitic limestones. Member 2 varies significantly and is characterized by red to purple interbedded mudstones and sandstones. Huang and Opdyke (2000) reported a thickness of 419 m for member 2 in the Badong and Nanzhang area, but found that this member was nearly twice that thickness (700 m) in the Sangzhi area (where the *Lotosaurus* Quarry is situated). However, Tang et al. (2009) reported member 2 as only reaching a thickness of 215 m in the Badong type area, noting that members 2 and 4 were both particularly prone to slip and landslides. Member 3 represents a thinly to thickly bedded limestone unit with a total thickness of 220–270 m (Huang and Opdyke 2000; Tang et al. 2009). Member 4 is similar to member 2, being characterized by red to purple siltstone and mudstone. Member 4 is reportedly between 356 m (Huang and Opdyke 2000) and 489 m (Tang et al. 2009) thick in the Badong area, but as thin as 250 m near Daxi and as thick as 850 m near Sangzhi (Huang and Opdyke 2000). Member 5 represents a dark gray dolostone that is no more than 25 m thick in the type area, but reaches ~ 200 m thick near Sangzhi (Huang and Opdyke 2000; Tang et al. 2006). It is important to note that Huang and Opdyke (2000) and Tang et al. (2009) reported nearly opposite thickness measurements for members 2 and 4 in the Badong type section. This area, like much of the Badong Formation, is strongly folded with numerous faults, and the potential for repeated section, blind thrusts, and other stratigraphic complications is high, particularly with respect to the lithologically similar members 2 and 4.

Age

The Badong Formation is generally considered to be Middle Triassic, primarily based on: (1) its stratigraphic position between better-dated Lower and Upper Triassic units (Zhang and Meng 1987); (2) biostratigraphic evidence from sparse marine invertebrates, primarily from the Badong type section (Zhang and Meng 1987); and (3) preliminary paleomagnetic studies by Huang and Opdyke (1996, 2000). Uncertainty surrounds the precise age of the deposits, with some workers suggesting a primarily Anisian age (e.g., Hounslow and Muttoni 2010), others suggesting an Anisian-Ladinian age (Zhang et al. 1987; Huang and Opkyke 2000), and others still suggesting the possibility that the formation covers most of the Middle Triassic and extends into the Carnian (e.g., Enos et al. 2006 and references therein). Zhang and Meng (1987) reported putatively Anisian invertebrate taxa from members 1 and 3 of the Badong type section, although Yin (2006) allowed that the ammonoid and bivalve fauna from member 3 could be Ladinian. Meng et al. (1995) and Meng (1996) studied the paleobotany of the Badong Formation in the Yangtze Gorge, north of our study area, and suggested an Anisian age for members 1–2 and a Ladinian age for members 4–5. Zhang and Meng (1987) also suggested that members 4–5 were most likely Ladinian, based on superposition.

Age estimates for the Badong Formation in other parts of the Yangtze Platform are mostly based on correlation with the type section, although it has been suggested that the formation may extend into the Carnian in Guizhou (Enos et al. 2006). Huang and Opdyke (1996, 2000) provided the best regional correlation of these deposits to date, as part of their preliminary paleomagnetic investigation of the formation. These authors presented a composite magnetozone stratigraphy for the Badong Formation based on partial datasets from three localities in Hubei and Hunan. However, a lack of calibrated tie points in these sections, as well as the clear potential for faulting and duplication of section, makes correlation to the global polarity time scale (GPTS) for the Middle Triassic challenging. This difficulty is implied by the alternative correlation of the Badong composite section with the Middle Triassic GPTS suggested by Hounslow and Muttoni (2010).

Depositional Environment

Facies and paleoenvironmental changes observed through the stratigraphy of the Badong Formation were primarily controlled by sea level cyclicity during closure of the Tethys Sea, as the SCC began docking with the NCC (Huang and Opdyke 2000). Most workers have suggested a shallow lagoonal to tidal flat setting (and possibly some fluvial intervals) for members 2 and 4 of the Badong Formation, whereas members 1, 3, and 5 have been interpreted as shallow marine shelf or platform carbonate sequences (Zhang et al. 1987; Meng et al. 1995; Huang and Opdyke 2000; and others). In Guizhou Province, workers have suggested that the Badong Formation was deposited mainly in a deeper water, turbidite-dominated terrigenous shelf-slope (flysch) environment, but that sub-aerial continental deposits may also have been present towards the east in particular (e.g., Enos et al. 2006 and references therein).

Zhang (1975) interpreted the *Lotosaurus* Quarry to be in member 2 of the Badong Formation, and suggested a lagoonal setting. Meng et al. (1995) and Meng (1996) suggested a tidal flat setting for member 2, and a storm tidal setting for the *Lotosaurus* Quarry (Meng et al. 1995). However, Liu (2016) recently described a new capitosauroid temnospondyl from member 2 of the Badong Formation in central Hubei Province, and

reported a continental setting with no evidence of tidal deposits. Indeed, sedimentological descriptions or interpretations are generally limited for the extensive Badong Formation, and comparatively little is known about the depositional environments or paleogeography, particularly from a regional perspective.

METHODS

In order to re-assess the age and stratigraphy of the *Lotosaurus* Quarry, we carried out a basic geologic investigation of the Sangzhi area. Strike and dip data from a series of outcrops were then plotted on a Google Earth image of the region, and used to identify the stratigraphic position of the bonebed. A detailed stratigraphic section was measured through the *Lotosaurus* Quarry and correlated to measured sections of the Badong Formation in the region by Huang and Opdyke (2000).

Paleogeographic reconstructions of the Badong Formation were produced in GPLATES V.16, based on the most recent global plate reconstructions of Matthews et al. (2016). The spatial distribution of the Badong Formation outcrops was compiled and imported into GPLATES as a shape file.

The newly excavated portion of the *Lotosaurus* Quarry was divided into 1 m^2 grid squares to facilitate mapping of the exposed skeletal elements. During the mapping process, we collected the following data: (1) identities of elements present; (2) length measurements for long, middle and short axes of elements; (3) orientations and plunges of elements; (4) presence or absence of modification features (e.g., tooth marks, insect borings) on elements; and (5) identities of any sedimentary structures present. A total of 975 elements were recorded and bone orientation data were analyzed to produce a traditional rose diagram in Stereonet 9, as well as a moving-average rose diagram generated by a MATLAB script (Munroe and Blenkinsop 2012). Fractal analyses of bone distribution randomness were also performed via a 'box-counting' method in ImageJ. This technique lays boxes of decreasing size around the edges of the bones in the bonebed to assess the density and complexity of bone groupings. Grouping was assessed across the entire suite of bones, as well as separately for each bone element type (e.g., appendicular).

Thin-sections were made of samples from bonebed-associated sandstone units to assess compositional and textural features. Laser-based grain size analyses were conducted on sediment samples from the bonebed via a Malvern Mastersizer 2000 at James Cook University (JCU). Clay mineral assemblage analyses were conducted on two bonebed samples (16-1-15-3 and 17-1-15-1A). Smear mounts of the recovered clay fraction for each sample were analyzed via XRD to determine the bulk clay content utilizing the PANalytical X'Pert Data Collector software. Three treatments were employed to assess the clay mineral assemblages following standard procedures: 'under air', ethylene glycol-solvation, and 'heating' (Moore and Reynolds 1997; Hillier 2003). A small amount of loose clay for each sample was also dried onto carbon double-stick tape on aluminum SEM stubs for SEM-EDS analysis on a JEOL 6610LV with an Oxford Instruments X-MAX Silicon drift energy dispersive x-ray spectrometer to corroborate the XRD results.

Two samples were collected for U-Pb detrital zircon geochronology: (1) sample 16-1-15-3, which was collected from a thin, medium-grained fluvial sandstone bed five meters above the bonebed; (2) sample 17-1-15-1A, which was collected from a medium-grained shoreline sandstone (foreshore facies) ~ 100 m above the top of the Badong Formation in the Upper Triassic Yingzuishan Formation, ~ 8 km west of the *Lotosaurus* Quarry near the village of Hongjiaguancun (Fig. 1). Both samples were prepared following the approach outlined by Tucker et al. (2013). Zircons were imaged by SEM cathodoluminescence to assess their zonation and structure, and to guide U-Pb intercoupled plasma mass spectrometry (ICP-MS; Bruker 820-MS) via laser ablation (Coherent GeolasPro 193 nm ArF Excimer; conducted at JCU). Instrument tuning and sample analysis followed the methodology outlined by Tucker et al. (2013). GJ-1 was used as the primary standard (609 Ma; Jackson et al. 2004) and Temora-2 (TEM-2; 416.8 Ma; Black et al. 2003) was used as the secondary standard. NIST 612 was analyzed at the beginning and end of each session to calibrate Th and U concentrations, as well as occasionally during data collection. The GLITTER software program (Van Achterbergh et al. 2001) was employed for data reduction and the data were assessed statistically using ISOPLOT (Ludwig 2012). All grains younger than 800 Ma were adjusted by a common Pb correction using the ISOPLOT function Age7Corr. Age determinations for zircon grains older than 1000 Ma were based on the Pb^{207}/Pb^{206} system, whereas those for younger zircons were based on the Pb^{206}/U^{238} system (Yan et al. 2011). A concordance filter of 15% was used for all grains older than 300 Ma. No filter was used for grains younger than 300 Ma due to the inherent problem with acquiring meaningful Pb^{207}/Pb^{206} ages on young grains (Gehrels 2012). In order to avoid biasing our results, different metrics were applied to calculate the maximum depositional age (MDA) of each sample following Dickinson and Gehrels (2009), Tucker et al. (2013) and Hilbert-Wolf et al. (2017).

Given that zircons sourced from different cratons can often be geochemically distinguished via Lu-Hf isotope analysis, we employed this technique on a representative population of detrital zircons in an attempt to narrow down their possible provenance. A total of 17 grains with concordant U-Pb ages, representing the main age peaks from sample 16-1-15-3, were selected for this analysis. The Lu-Hf analysis was conducted using a coupled Thermo Scientific Neptune multicollector (MC) ICP–MS and GeoLas Pro 193 nm ArF Excimer at JCU. Analytical protocols and methods followed those established by Kemp et al. (2009) and Næraa et al. (2012). See also Tucker et al. (2016) for a more detailed description of laboratory methods and data processing.

RESULTS

Stratigraphy

The total thickness of the Badong Formation is estimated to be ~ 2000 m in the Sangzhi area (Huang and Opdyke 2000). In the field, a gradational contact between the top of member 1, characterized by a series of petroliferous-smelling, thin gray to slightly reddish calcareous shales, and the base of member 2 was identified. Because most of member 2 in the study area at Furongqiao is covered by vegetation, the stratigraphic height of the bonebed was calculated based on field measurements of strike and dip between the top of member 1 and the bonebed. The *Lotosaurus* Quarry sits near the top of member 2, ~ 750 m above the base of the formation, which is consistent with the original stratigraphic interpretation by Zhang (1975). This finding is also consistent with thicknesses of members 1 and 2 reported by Huang and Opdyke (2000) from a locality ~9 km NW of Sangzhi.

Sedimentology

The site is characterized by a short, but well-exposed, section of steeply dipping maroon mudstones and sandstones. Strata above and below this interval are mostly covered by vegetation, although isolated exposures are abundant in the area, particularly along small streams and road cuts. The ~ 40 m thick measured section through the *Lotosaurus* Quarry starts with a basal 10 m-thick upward-coarsening succession, which is succeeded by two 10 m-thick upward fining depositional cycles (Fig. 2). Paleocurrent measurements taken on cross-bedding and abundant flute and groove casts at the bases of sandstone bodies throughout the section containing the *Lotosaurus* Quarry ($n = 33$) indicate southwest flow direction (vector mean = 250.2°; Fig. 2).

Seven different facies are recognized in member 2 of the Badong Formation, five of which crop out in the *Lotosaurus* Quarry section. These include the following: horizontally laminated red mudstone to muddy

Furongqiao Section

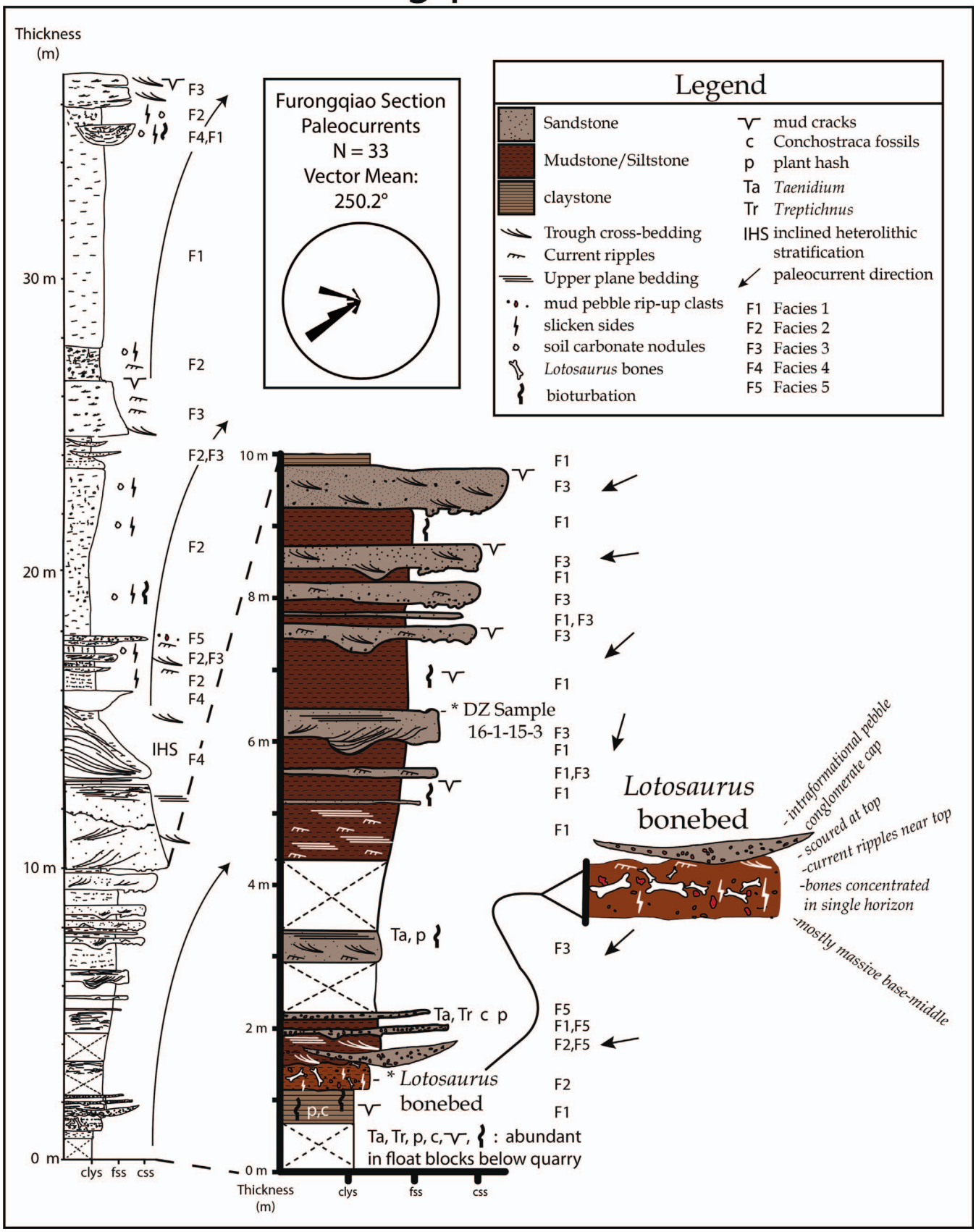

TABLE 1.—*Descriptions of the various facies recognized within the Badong Formation outcrop at the* Lotosaurus *Quarry*.

Facies Code	Facies Description	Diagnostic Features	Fossils	Interpretation
F1	Horizontally laminated, red muddy sandstone to mudstone	Horizontal laminations; weak upward fining; sub-cm scale wave & current ripples present locally; small-medium mudcracks common	Minor bioturbation; Mottled rootlets; concostrachans; plant hash, leaves & stems; *Lotosaurus* Quarry	Low-energy sedimentation in floodplain ponds/depressions, lakes, or abandoned channels; cyclic wetting & drying cycles
F2	Massive, red mottled mudstone to muddy sandstone	Massive w/ intense bioturbation; abundant small $CaCO_3$ nodules & slickensides; blocky ped structures; mottling	Intense bioturbation; rhyzo-concretions	Pedogenically modified floodplain deposits-Vertisols; seasonal to semi-arid setting
F3	Current ripple cross laminated to horizontally laminated sheet sandstone	Sheet like sandstones; localized channel-form architecture; basal flute & groove casts; current ripples; planar lamination; weak upward fining; mudcracks & burrows at top of beds	Rootlets; burrows: *Treptichnus* sp. & *Taenidium cameronensis*	Crevasse-splay and small crevasse channels, or tributary streams
F4	Thick, trough cross-bedded to planar laminated lenticular sandstone	Small-medium scale trough cross-bedding; planar bedding w/ parting lineations; basal flute casts and erosional scour; 1-2 m scale lateral accretion surfaces & inclined heterolithic stratification	Burrows; plant hash	Small-medium sized meandering fluvial channels; possibly tidally influenced
F5	Thin, lenticular intraformational pebble conglomerates	Conglomerate dominated by intra-formational mudstone rip-up clasts & calcium carbonate nodules eroded from underlying units; minor trough cross-bedding	Na	Flood-related channel incision & sheet flooding
F6	Horizontally laminated mudstone w/ large-scale desiccation cracks	Clay-rich mudstone w/ meter-scale mudcracks; laterally extensive; mottling & local reduction halos	Na	Tidal flat, lacustrine or floodplain
F7	Wave-ripple laminated, lenticular sandstone	Normal grading; small mudcracks	Abundant burrows; vertebrate bones	Tidal flat, lacustrine or floodplain

sandstone (F1); massive, mottled mudstone and muddy sandstone with calcium carbonate nodules (F2); thin, horizontally laminated to ripple cross-laminated sheet sandstone (F3); thick, cross-bedded to planar laminated lenticular sandstone (F4); thin, lenticular intraformational pebble conglomerates (F5; Table 1). Several other facies were also documented in member 2 from other sections, including laminated mudstone with large-scale desiccation cracks (F6) and wave-ripple laminated, lenticular sandstone beds (F7). Details of the lithology and interpretation of each facies are summarized in Table 1.

The *Lotosaurus* Quarry is situated at the base of the measured section (Figs. 2, 3), although loose blocks and small outcrops just below the bonebed unit preserve mud cracks and conchostrachan fossils. Directly above this, outcrop and thin section analysis of the bone-bearing unit demonstrates that it represents a combination of massive to horizontally laminated muddy, very fine-grained sandstone to mudstone with relatively poor sorting (F1 and F2), and is 20–23 cm thick. Thin-section analysis also indicates sub-angular to sub-rounded grains with roughly the following modal percentages: monocrystalline quartz $\sim$ 70–80%, lithic sedimentary grains $\sim$ 10–20% and potassium feldspar $\sim$ 5–10%. The geometry of the bonebed is difficult to fully assess due to limited exposure, but the bonebed is generally tabular ($<$ 20 cm thick) and extends a minimum of 20–30 meters laterally and a minimum of $\sim$ 10 m in the orthogonal direction (E-W). Bones are primarily flat-lying and concentrated at the top of this unit, but in one area several bones are aligned vertically and appear to penetrate lower into the deposit. Indistinct bioturbation, small-scale slickensides and small calcium carbonate nodules ($<$ 2 cm in diameter) characterize much of the bone-bearing interval, but these features are largely absent from the top few centimeters of the bonebed. Instead, the uppermost 7 cm of the bonebed interval is less muddy, and displays current ripples and very small-scale trough cross stratification (F3). The current ripples in this interval are up to 7 cm thick, and preserve evidence of internal scour. Roughly 5–8 cm above the top of bonebed, a distinctive 3–5 cm-thick intraformational pebble conglomerate (F5) is exposed. This conglomerate is composed primarily of small calcium carbonate nodules, similar to those found lower in the bonebed.

The 15 m stratigraphic interval immediately above the *Lotosaurus* Quarry is dominated by horizontally laminated mudstones and siltstones (F1) and thin ($<$ 45 cm thick), horizontally laminated to ripple-cross laminated sheet sandstones (F3) that show rill marks and evidence of episodic current flow, bioturbation, and desiccation. This interval is capped by a 3 m thick cross-bedded sandstone unit (F4), overlain directly by a 1.5 m thick sandstone unit (F4) that displays large-scale inclined heterolithic stratification. Internal scour surfaces in both units are characterized by the presence of rip-up clasts, whereas their upper surfaces preserve abundant very small-scale current ripple cross-laminations, including climbing ripples in places. Occasional thin lenticular beds of intraclast pebble conglomerate (F5) are present within F1 and F2, particularly just above the bonebed interval. Both the thick and thin sandstone beds (F3, F4) in this interval are typified by flute casts and evidence of basal erosional scour along their bottom contacts. Upper contacts, particularly for F3, typically

←

FIG. 2.—Measured section through the Badong Formation of Furongqiao Township, in the immediate vicintity of the *Lotosaurus* Quarry, with detail of interval surrounding bonebed. The entire measured section is part of member 2 of the Badong Formation and is characterized by a fluvial and floodplain succession. The positions in the section of the bonebed and detrital zircon sample site are indicated. Unidirectional paleocurrent measurements taken from outcrop exposures are also shown (black arrows).

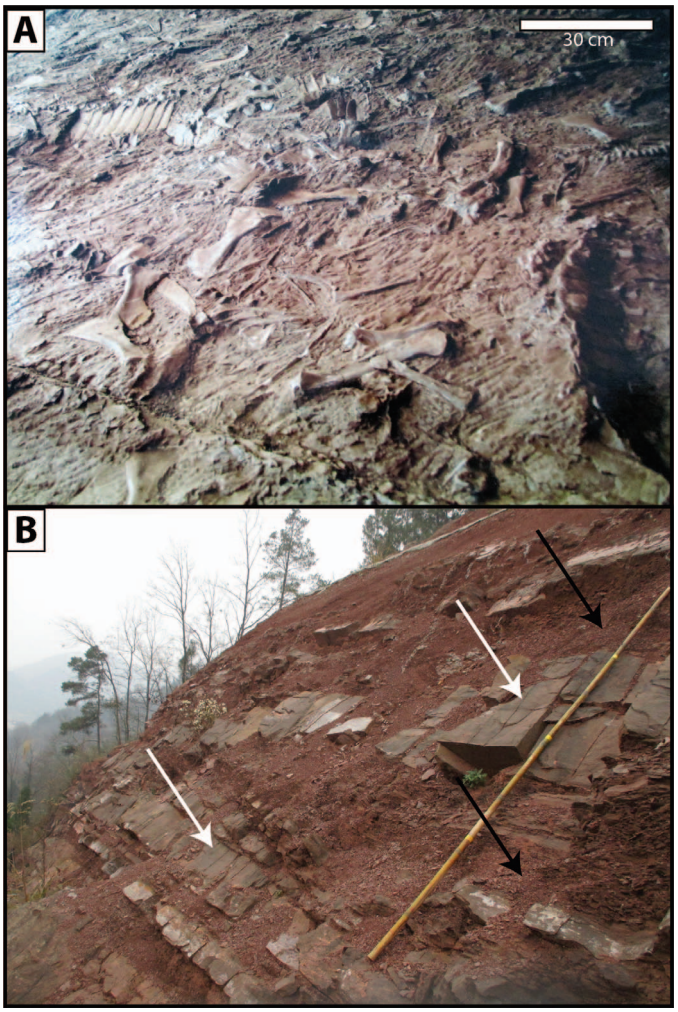

FIG. 3.—Photographs of the *Lotosaurus* Quarry bonebed and stratigraphic section. **A**) Excavated bone bed showing dense concentration of *L. adentus* bones. **B**) Outcrop view of dipping strata of the Badong Formation (member 2); note the large-inclined foresets in the bottom of the photo (indicated by white arrows), which are interpreted as a channel point bar succession overlain by repeated channel sandstones and overbank mudstones (indicated by black arrows). Scale: staff is 2 m long.

preserve small to medium-scale desiccation cracks. Plant hash, large, whole leaves, and conchostrachan fossils are locally present within thin (< 2 cm-thick) green siltstone horizons (F1) situated near the base of this interval, a few meters above the bone bed level. Meng et al. (1995), who referred to this area as Lotus Bridge (a translation of "Furongqiao"), reported a high diversity of plants, including *Pleuromeia*, *Annalepis*, *Calamites*, and *Equisetites*. Bioturbation is common in this part of the section, ranging from intense bioturbation in F1 to exceptionally preserved examples of burrows, including *Treptichnus* isp. and *Taenidium cameronensis*, in F2, F3 and F4 (Fig. 2).

Above this level (~ 15 m above the bonebed), the strata become distinctly finer grained, and dominated by mudstone and muddy sandstone (F1 and F2). Massive mudstones and sandstones (F2) with mottling, burrows, roots, and small calcium carbonate nodules characterize most of the uppermost 18 m of the local section. Thin current ripple cross-laminated sandstones are also present in this part of the section. High in section, a distinct, lenticular channel-form element is filled almost entirely with massive mudstone containing calcium carbonate nodules, slickensides, mottling and burrow/root networks. No fossils, apart from rootlets and indistinct burrows, were found in this upper interval.

Taphonomy of the Lotosaurus *Quarry*

The total number of *L. adentus* bones recovered during the original and subsequent bonebed excavations in the 1970s and 1980s is uncertain, but extended into the hundreds, and Zhang (1975) estimated the minimum number of individuals from the original excavations in 1970 and 1981 to be more than ten. Of the two specimens figured in his paper, IVPP (Institute of Vertebrate Paleontology and Paleoanthropology, Chinese Academy of Sciences, Beijing) V4881 was a small, mostly intact skull, and IVPP V4880 was an incomplete, partially articulated skeleton comprising most of the presacral vertebrae together with some ribs and appendicular elements. In 2012, a large additional area (~ 90 m^2) of the bone layer was excavated, although almost all the exposed skeletal elements were left in place. Despite this renewed quarrying effort, areas containing densely concentrated bones still remain to be excavated both laterally across the face of the hill and down dip into the subsurface. Almost all the skeletal elements ever exposed in, or collected from, the *Lotosaurus* Quarry seem to pertain to *L. adentus*. However, two isolated teeth, one belonging to a temnospondyl and one to a carnivorous archosauriform, were recovered during the 2012 excavations. Zhang (1975) also reported that an equisetalean fossil and a "nothosaur" dorsal vertebra and fibula, closely comparable to the equivalent bones in *Chinchenia sungi* from the Middle Triassic Guanling Formation of Guizhou, had been found together with the *L. adentus* bones during the original excavations. *Chinchenia sungi* is now regarded as a basal pistosauroid sauropterygian (Rieppel 1999; Li et al. 2008). However, these putative sauropterygian bones from the *Lotosaurus* Quarry cannot presently be located, and may have been misidentified.

In 2015, we returned to the *Lotosaurus* Quarry to map and document the exposed, in situ bones, cataloging 975 elements, all but two of which pertain to *L. adentus* (Fig. 4; online Supplemental File, table S1). At a minimum, 274 of the 975 bones mapped in the quarry (~ 28%) are articulated. We estimate that the bones mapped in 2015 represent a minimum of 28 individuals, based on the presence of 55 identified scapulae. However, estimates would be considerably higher (> 38) if the specimens collected in the 1970s and 1980s were included. A minimum of five partial skeletons are known to have been reconstructed from these earlier excavations, including three skeletons excavated in 1981 by the Hunan Geological Museum, which were sent to various museums and collections in China. The degree of articulation and completeness of these specimens is unknown, but the nature of the material we observed at the *Lotosaurus* Quarry suggests that each reconstructed skeleton must have been cobbled together from disarticulated bones and strings of articulated elements collected in the bonebed.

Following the modified Voorhies (1969) group classification of Gates (2005) for dinosaurs, we classified bones into Voorhies Groups I and II to examine the potential for hydraulic sorting. The results suggest that a moderate degree of hydraulic sorting likely occurred at the site following the deaths of the individuals. Specifically, the site shows a disproportionately high number of Group II elements and a general paucity of certain Group I elements (e.g., phalanges, hemal arches). The over-representation of ribs and vertebrae (Group I) is due to the high degree of articulation in many of these elements, which would have caused them to behave hydraulically like Group II elements. This pattern of hydraulic sorting is supported by a reasonably strong degree of preferential bone orientation (*in situ* bone measurements provide a bidirectional vector mean of 78.1°–258.1°; Fig. 4). Fractal analysis of the quarry also suggests that the bone distribution is non-random, and that there are distinct groupings of bones across the bonebed. The fractal dimension (*D*), essentially a measure of complexity or the efficiency of space utilization, is ~ 1.6 for the entire bonebed. Analyses were also conducted on each bone element type: axial

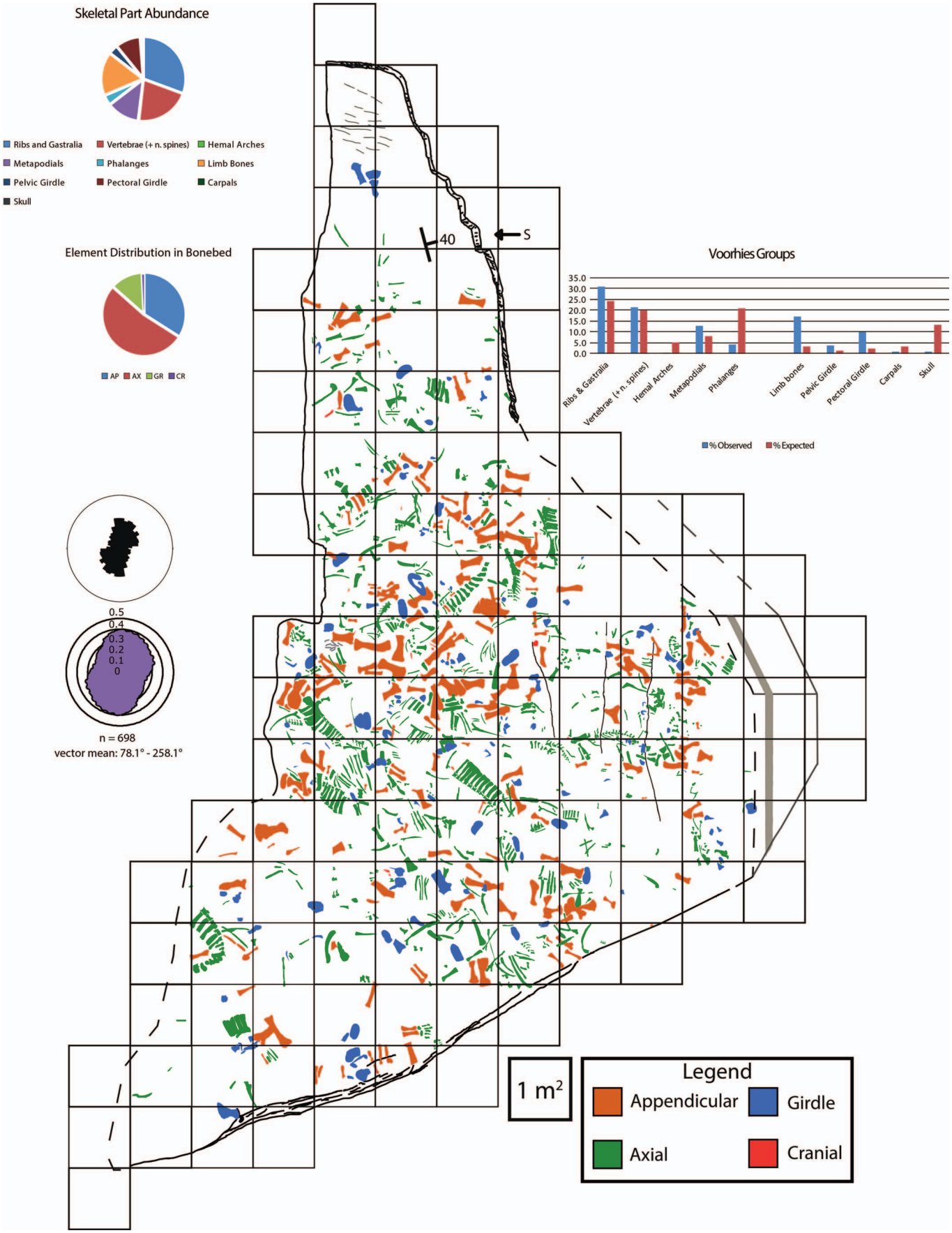

FIG. 4.—Digitized bonebed map of the *Lotosaurus* Quarry. The black rose diagram shown on the left was created utilizing traditional methods, whereas the purple rose diagram on the right was created utilizing a moving average method. Girdle elements in blue, cranial elements in red, appendicular elements in orange, and axial elements in green.

bones yielded $D \sim 1.2$; appendicular bones yielded $D \sim 1.2$; girdle elements yielded $D \sim 1$. A value of $D \sim 1$ indicates bones are evenly spaced with no dominant grouping, whereas a D value > 1 indicates greater distributional complexity, bone density, and efficiency of space utilization. Both axial and appendicular bones exhibited grouping throughout the bonebed, whereas the girdle elements tended to be roughly evenly spaced. There were too few cranial elements to provide a meaningful D value (Fig. 5).

Axial and appendicular elements were most common in this assemblage ($\sim$ 51% and $\sim$ 35%, respectively), although occasional girdle elements ($\sim$ 13%) and rare cranial elements (n = 7; $\sim$ 1%; Table 3) were also present. Cranial elements appeared to be the least intact, with most showing evidence of damage, whereas axial elements exhibited the greatest level of articulation and the least damage. Partially articulated vertebral columns were often found with associated girdle and limb elements.

Comparisons of the long-axis measurements of different appendicular and girdle elements reveal a considerable amount of variation in body size among the individuals represented in the bonebed. For instance, the length of the largest intact femur measured 42 cm and the smallest intact femur measured 18 cm; with a broad distribution of values within that range (see online Supplemental File). Similar patterns are observed for the other appendicular and girdle elements, indicating that the bonebed contains individuals that vary widely in size.

Bone modification features across the bonebed were exceedingly minimal, with most elements in excellent condition. Bone weathering in the bonebed was predominantly recorded as 0 (e.g., no weathering evident) out of 3 on the Behrensmeyer (1978) bone weathering scale, but some elements, particularly the cranial ones, did appear to have undergone more weathering (typically $\sim$ 1). None of the excavated bones exhibited any evidence of predation, scavenging, insect modification, or trampling damage. Minimal evidence of abrasion was present (predominantly 0–1; sensu Fiorillo 1988). Qualitative observations of bone breakage patterns revealed minimal evidence for green stick fractures or other types of trauma or pathology.

Clay Mineralogy

The XRD analyses revealed clay mineral assemblages containing kaolinite, illite, vermiculite, and quartz in samples 16-1-15-3 and 17-1-15-1A (Fig. 6). There may have also been trace amounts of other clay minerals in the interlayers (potentially montmorillonite), but we were unable to verify additional clay minerals in our analyses. Kaolinite seemed to be highly abundant, whereas there was only a small amount of illite and even less vermiculite. SEM-EDS results corroborated those from the XRD analyses (Fig. 6).

Detrital Zircon Geochronology
Sample 16-1-15-3

Sample 16-1-15-3 consisted of 189 grains, 128 of which were found to be concordant, with ages ranging from 225.6 Ma to 2876.3 Ma (Fig. 7; online Supplemental File, table S2). The age distribution of the grains was as follows: 41 grains (32%) of 200–350 Ma; 10 grains (8%) of 350–400 Ma; 31 grains (24%) of 400–650 Ma; zero grains of 650–700 Ma; 26 grains (20%) of 700–1200 Ma; four grains (3%) of 1200–1550 Ma; 10 grains (8%) of 1550–2050 Ma; two grains (1.5%) of 2050–2300 Ma; two grains (1.5%) of 2300–2600 Ma; two grains (1.5%) of $>$ 2600 Ma.

Sample 17-1-15-1A

Sample 17-1-15-1A consisted of 64 grains, 39 of which were found to be concordant, with ages ranging from 248.5 Ma to 2432.1 Ma (Fig. 7; online Supplemental File, table S3). The age distribution of the grains was as follows: 14 grains (48%) of 200–350 Ma; six grains (15%) of 350–400 Ma; four grains (10%) of 400–650 Ma; zero grains of 650–700 Ma; nine grains (23%) of 700–1200 Ma; zero grains of 1200–1550 Ma; three grains (8%) of 1550–2050 Ma; one grain (2.5%) of 2050–2300 Ma; two grains (5%) of 2300–2600 Ma; zero grains of $>$ 2600 Ma.

Detrital Zircon Lu-Hf Analysis

The Lu-Hf isotope results from the group of zircon populations analyzed in sample 16-1-15-3 showed a wide spread of initial $^{176}Hf/^{177}Hf$ ratios, ranging from 0.281368 to 0.282844, while εHf(t) values ranged from –43.5 to +8.2 (Fig. 8A, 8B; online Supplemental File, table S2). Most grains (n = 14) produced negative initial εHf(t) values. Generally, zircons yielding positive initial εHf(t) values are indicative of juvenile crustal additions/growth or significant input from depleted, newly melted upper mantle material with minimal reworking, whereas negative εHf(t) values indicate crustal reworking (Morag et al. 2011). The dominant negative εHf(t) values from this study are thus consistent with reworked crustal sources for the zircons. Hf isotopic model ages (T_{DM}) obtained for the studied zircons ranged from ~2621.8 Ma to 614.2 Ma.

Metcalfe (2013) presented a compilation of zircon Hf model ages from sources in the SCC, NCC, and Tarim Block, which showed relatively distinct trends in Hf model ages associated with the different tectonic blocks (Fig. 8C). It was hoped that, given the distinct separation between the NCC and the SCC Hf model ages, this investigation of Lu-Hf model ages of detrital zircons from sample 16-1-15-3 might provide additional insight into sediment provenance. However, our results indicate a much younger and broader range of Hf model ages than would be expected for zircons from either source.

INTERPRETATIONS AND DISCUSSION

Geological Age of Lotosaurus adentus

The first objective of the detrital zircon study was to try to refine the age of *L. adentus* by determining the maximum depositional age (MDA) of sample 16-1-15-3. MDA can be assessed using many different approaches (e.g., Tucker et al. 2013; Hilbert-Wolf et al. 2017), the simplest of which is to base the age estimate on the youngest single grain (YSG) in the sample. However, many studies have emphasized the hazards of using the age of any single grain to assess MDA. The most serious issue with this approach is the potential for zircons to experience Pb loss due to cracks, metamorphism or other factors, leading to artificially young ages. Thus, a combination of different approaches is typically applied (Fig. 7; Table 4), with the most robust approaches typically based on weighted averages or plotting the lower intercept of the youngest 'natural', coherent grouping of grains (Dickinson and Gehrels 2009). The risk associated with using a weighted mean or lower intercept age is that the youngest apparently 'natural' population may in fact represent more than one distinct zircon population, leading to an MDA that is too conservative (older than the true MDA; Dickinson and Gehrels 2009). Another way to estimate MDA is to simply take the youngest peak population (YPP) age from the frequency distribution diagram (Dickinson and Gehrels 2009). However, there is no single ideal method for calculating an MDA from a population of detrital zircons, and data must be evaluated both statistically and geologically.

In the case of sample 16-1-15-3 (from five meters above the *L. adentus* bonebed), the results were fortuitous in that a suite of five young, potentially age-constraining detrital zircons could be identified (Fig. 7; online Supplemental File, table S3). The YSG age is 225.6 Ma, which is considerably younger (Norian: 227–208.5 Ma) than previous estimates for the bonebed by Zhang (1975) and others. If we include this grain in the age calculations, the YPP is 232 Ma, the weighted mean age of the youngest coherent population (e.g., the 225.6 Ma grain plus the next youngest four grains) is 233.6 ± 8.3 Ma, and a lower intercept solution on the Terra-

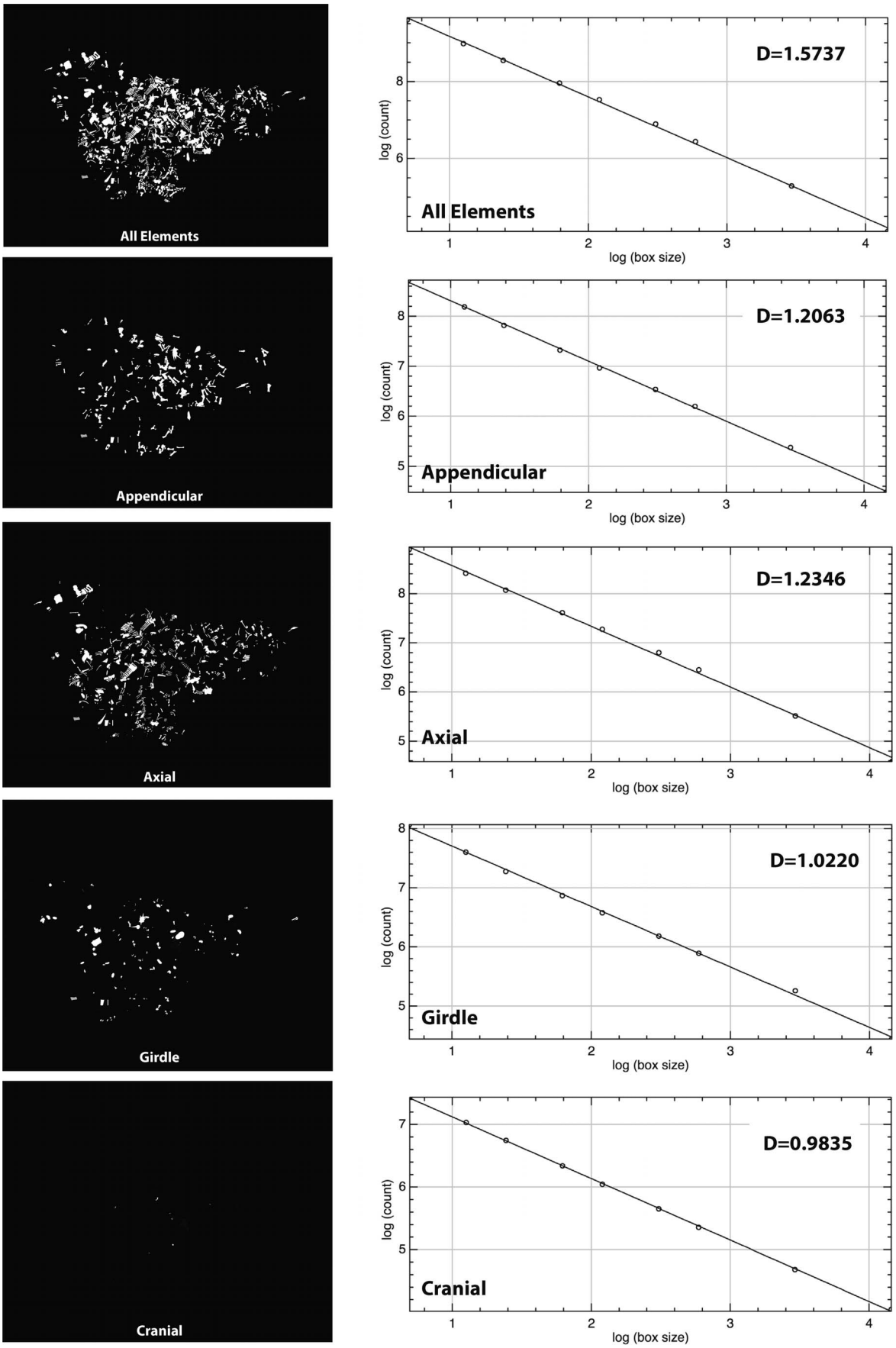

FIG. 5.—Results of fractal analysis on the bonebed maps with accompanying plots showing 'box-counting' results. The fractal dimension, *D*, is the slope of the linear regression (between log[box size] and log[box count]) plotted. These fractal analyses were conducted with a built-in box-counting routine in ImageJ.

TABLE 2.—*Bonebed element data for MNE and MNI assessment. Abbreviations: AP = appendicular; AX = axial; CR = cranial; GR = girdle. Asterisk indicates that the number of individuals varies by species, unknown for* L. adentus.

Element	MNE	MNI	Type
Astragalus	12	3	AP
Calcaneum	11	3	AP
Carpal	5	1	AP
Centrum	14	*	AX
Chevron	3	*	AX
Clavicle	1	1	GR
Coracoid	17	9	GR
Femur	29	15	AP
Fibula	36	18	AP
Frontal	1	1	CR
Gastralia	26	*	AX
Humerus	24	12	AP
Ilium	3	2	GR
Interclavicle	5	5	AX
Ischium	19	10	GR
Mandible	4	2	CR
Metacarpal/Metatarsal	100	5	AP
Neural spine	64	*	AX
Occipital condyle	1	1	CR
Phalanx	39	1	AP
Pubis	13	7	GR
Qudratojugal	1	1	CR
Radius	20	10	AP
Rib	272	*	AX
Sacrum	1	1	AX
Scapula	55	28	GR
Scapulocoracoid	16	8	GR
Tibia	31	16	AP
Ulna	24	12	AP
Vertebrae	128	*	AX

* Number per individual varies by species, unknown for L. adentus

Wasserberg Concordia diagram yields an age of 230.6 ± 5.6 Ma (Fig. 7). However, if we reject the youngest (225.6 Ma) grain in the sample, the youngest remaining grains that form a coherent grouping are a cluster of four. If these four grains are used as a basis for calculations, the weighted mean age and lower intercept solution both become slightly older (236.3 ± 8.0 Ma [1σ] and 234.1 ± 4.8 Ma [1σ], respectively) (Fig. 7). More importantly, the mean squares weighted deviation (MSWD) values for the weighted mean age and lower intercept solution drop significantly from 5.1 and 1.2 to 2.7 and 0.68, respectively (Fig. 7). This significant improvement in the MSWD of the sample might suggest that two populations are represented in the five youngest grains, but we interpret this as evidence of probable Pb-loss in the YSG, making it distinct from the other young grains. Therefore, our preferred solution is to reject the 225.6 Ma grain and base our final MDA interpretation on the other four young grains. Using these grains, the lower intercept age of 234.1 ± 4.8 Ma gives a better MSWD (0.68) than the weighted mean age of 236.3 ± 8.0 Ma and is also associated with lower uncertainty, suggesting the lower intercept age is more reliable (Fig. 7).

In summary, we interpret the MDA of sample 16-1-15-3 to be 234.1 ± 4.8 Ma, although we cannot rule out the more conservative weighted mean age of 236.3 Ma ± 8.0 Ma. This suggests that *L. adentus* most likely lived in the Carnian (237–227 Ma) or Ladinian (242–237 Ma), rather than in the Anisian (247.2–242 Ma) as previously thought. Because of the large uncertainty associated with the age estimate, an end-Anisian age cannot be ruled out at present. The MDA obtained for the *Lotosaurus* Quarry must be viewed with caution, but the balance of evidence does suggest that the bonebed, and hence the top of member 2 of the Badong Formation, is likely younger than Anisian, probably Ladinian, but perhaps even as young as Carnian. This Ladinian/Carnian age is more consistent with the phylogenetic position of *L. adentus*, which appears to be nested within a clade of Late Triassic derived poposauroids known from North and South America (Nesbitt 2007, 2011). Our results also broadly agree with published magnetostratigraphic ages (Huang and Opdyke 2000) (Fig. 9), bolstering our confidence that the *Lotosaurus* Quarry is indeed Ladinian or Carnian.

TABLE 3.—*Bonebed element composition. Abbreviations: AP = appendicular; AX = axial; CR = cranial; GR = girdle.*

	Total	Percentage
Total	975	100
AP	331	33.9
AX	513	52.6
GR	124	12.7
CR	7	0.7

Depositional Environments and Paleoclimate of the Lotosaurus *Quarry*

Outcrops of the Badong Formation at the *Lotosaurus* Quarry contain many sedimentary structures, including cross-bedding, climbing ripples, upper-plane bedding, flutes and rip-up clasts, as well as evidence of point bar lateral accretion. These sedimentary structures are all consistent with a fluvial-floodplain depositional environment, although the heterolithic nature of the point bar lateral accretion suggests possible tidal influence on the fluvial system (see Table 1 for specific interpretations of each facies). In addition, the section contains abundant continental trace fossils (including root traces), mudcracks, and paleosols both above and below the quarry level. All these features are consistent with a continental floodplain environment, but inconsistent with the lagoonal setting proposed by Zhang (1975). However, in fairness, the 40 m section that was available for us to study the sedimentology of the site was only exposed in 2012 after the bonebed was reopened and excavators were used to build the large shelter over the site. Prior to this, the site would have been densely vegetated, and Zhang's (1975) paleoenvironmental interpretations were presumably based largely on nearby sections in Sangzhi city and in the Yangtze Gorge that do expose lagoonal and tidal flat facies (see Meng et al. 1995; Huang and Opdyke 1996; Meng 1996).

Some additional paleoclimatic inferences can be made for this locality based on clay mineral assemblage analyses interpreted in light of the estimated paleolatitude. The relatively high abundance of kaolinite, with lesser amounts of illite and even less vermiculite, in both samples is consistent with a subtropical climate with relatively low mean annual precipitation (MAP) values of 100–150 cm and intermediate levels of weathering (Dixon and Weed 1989; Birkeland 1999). The presence of small calcium carbonate nodules, weak to moderate soil horizon development, roots, slickensides and blocky ped structures in certain beds is consistent with vertic paleosol development (vertisols) under seasonally wet-dry conditions. Conchostracan fossils occur above and below the bonebed. These animals require that their eggs dry out as part of the cycle between laying and successful hatching, which requires an environment with fluctuating wet-dry conditions (A. Stigall, personal communication). For this reason, conchostrachans are commonly, although admittedly not exclusively, associated with semi-arid settings hosting ephemeral streams and lakes (Webb 1979). The occurrence of associated mudcracks in these facies is consistent with this type of environment. The presence of plant hash, whole leaves and stems in the lower part of the *Lotosaurus* Quarry sections indicates that seasonal or occasional wet periods also occurred.

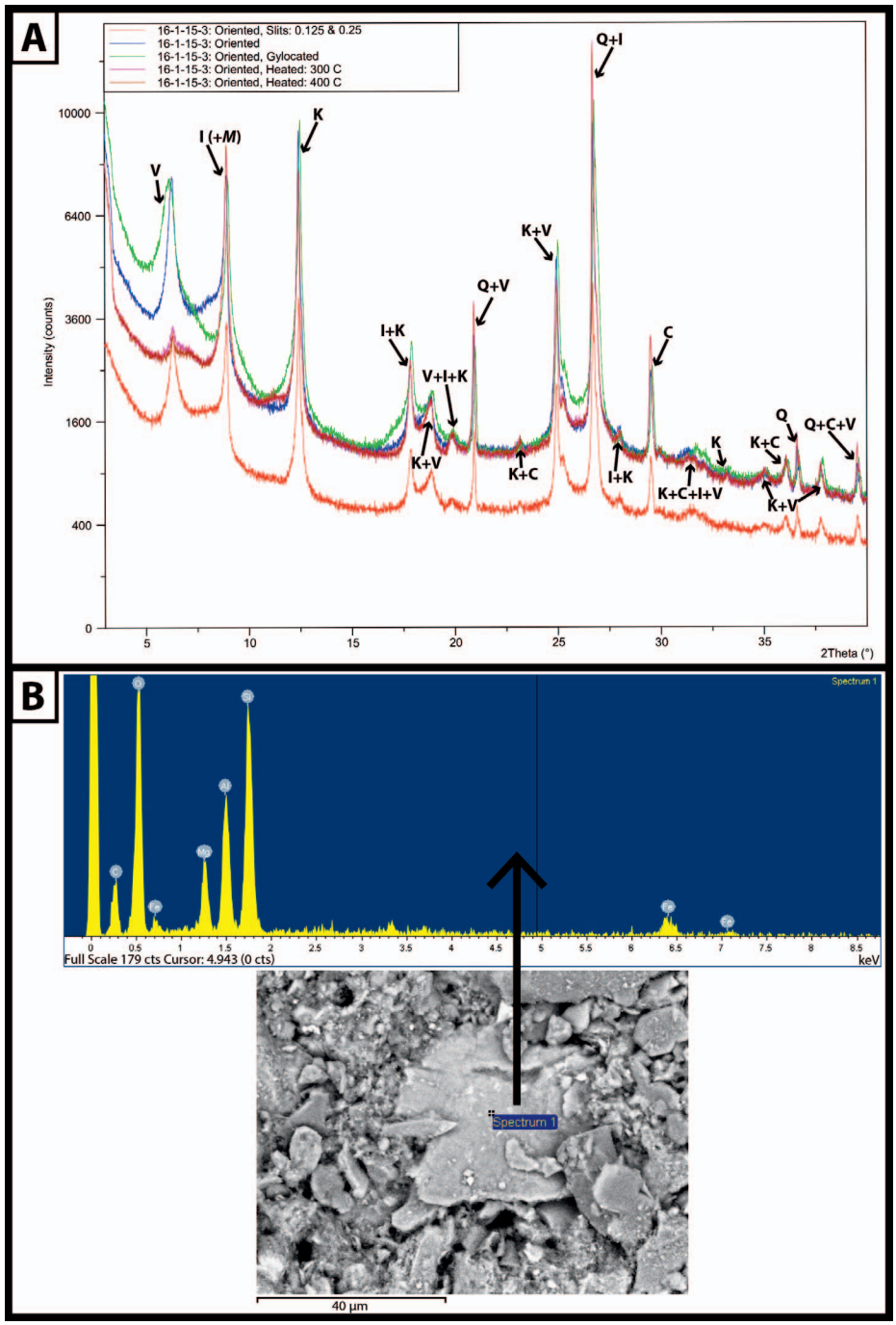

FIG. 6.—**A**) XRD analysis of sediment collected from above the *Lotosaurus* Quarry (Sample 16-1-15-3). Fixed divergence and anti-scatter slits are ⅛° and ¼° (red), and ¼° and ½° (blue, green, pink, brown). Green curve produced after glycolation; pink and brown curves produced after heating (300°C and 400°C, respectively). Peaks labeled as follows: V = vermiculite; I = illite; K = kaolinite; C = calcite; Q = clay-sized quartz; M = montmorillonite. **B**) SEM-EDS spectrum and SEM image of sediment collected from above the *Lotosaurus* Quarry (sample 16-1-15-3).

These findings are consistent with paleogeographic reconstructions that have the SCC moving through the subtropics during the Middle Triassic (Matthews et al. 2016). The *Lotosaurus* Quarry would have been located at ~ 34° N latitude by 235 Ma (Fig. 10). Considered together, the available evidence points to a hot climate with periodic, seasonality, or short-term variability in water availability during the deposition of the *L. adentus* bonebed.

Taphonomy and Formation of the Lotosaurus *Quarry*

The *Lotosaurus* Quarry is located within a fluvial-floodplain succession characterized by small, meandering-channel sandstones; shallow, ephemeral pond–lake mudstones; weakly developed vertic paleosols; and thin crevasse splay sandstones derived from sediments deposited on the adjacent floodplains (see Table 1 for details). This suite of features implies a pattern of channel flooding, which resulted in sedimentation and ponding

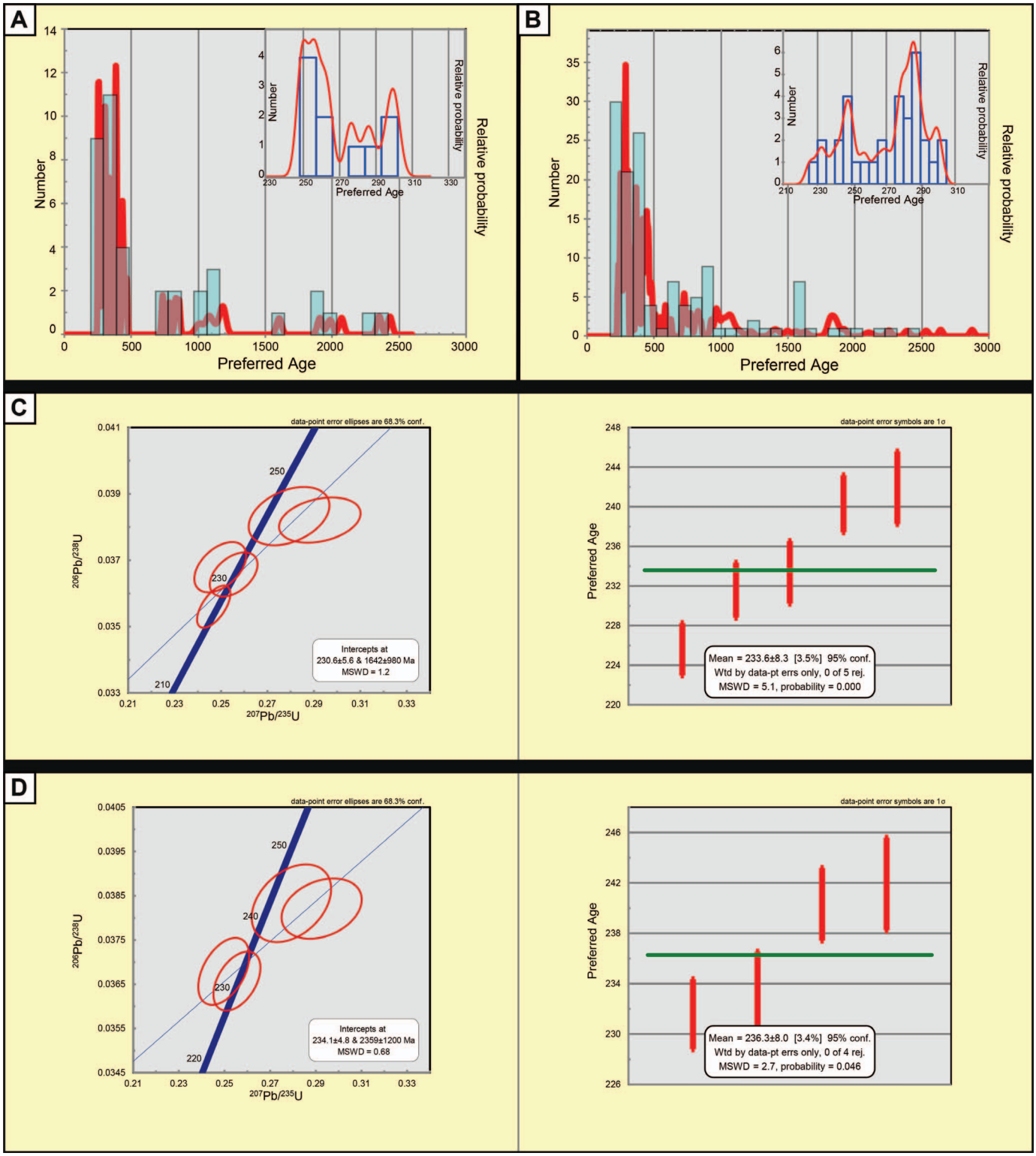

FIG. 7.—**A**) Probability density plots of zircon ages for sample 17-1-15-1A. Blue columns are age bins of 100 million years. **B**) Probability density plots of zircon ages for sample 16-1-15-3. Blue columns are age bins of 100 million years. **C**) Concordance and age distribution plots of the five youngest grains measured from sample 16-1-15-3. **D**) Concordance and age distribution plots of the four youngest grains, excluding the youngest measured grain, from sample 16-1-15-3.

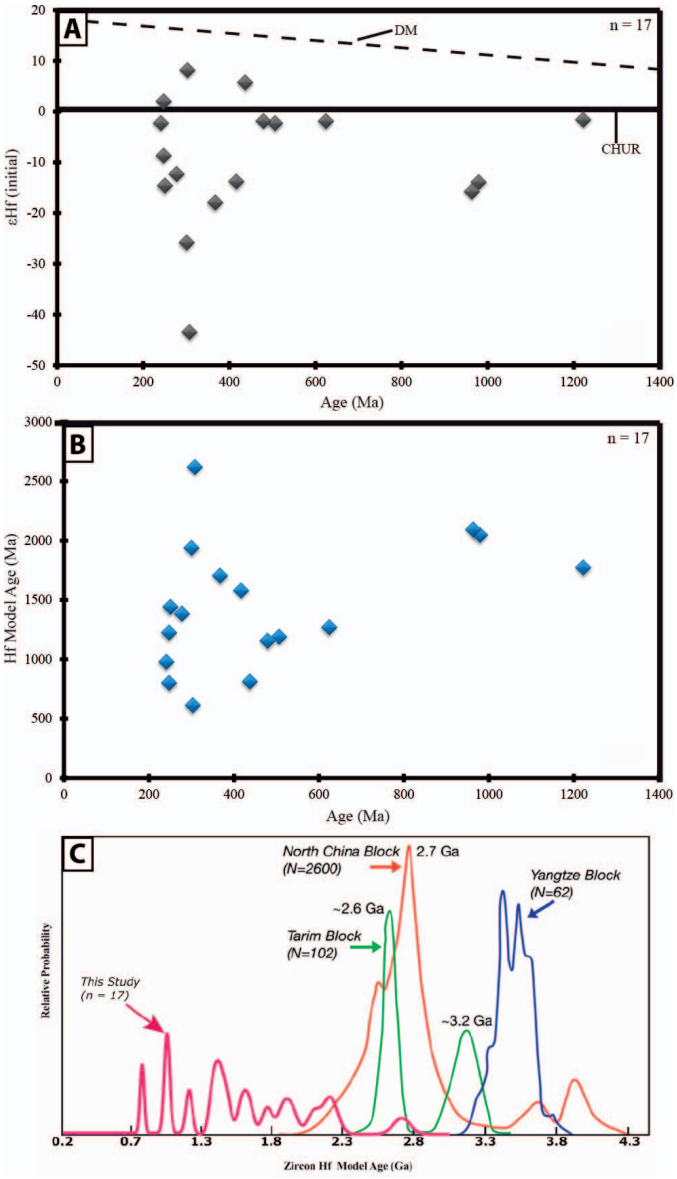

FIG. 8.—Hafnium isotope results and model ages from this study and previous work. **A**) Plot of initial εHf values vs U-Pb ages of concordant detrital zircons from sample 16-1-15-3. **B**) Plot of Hf model ages vs U-Pb ages, showing that most zircons in this study were derived from reworked crustal sources. Depleted mantle (DM) evolution curve is for linear evolution from a Chondritic Uniform Reservoir (CHUR) value at Earth's formation (0 at 4.56 Ga) to εHf(t) = 17 at present (Dhuime et al. 2011). **C**). Zircon Hf model age spectra modified from Metcalfe (2013), Geng et al. (2012), and Long et al. (2010). Hf data from this study are plotted in pink and primarily indicate a recycled craton origin.

on the floodplain and was followed by desiccation and soil development. Closer inspection of the bonebed itself suggests that skeletons of dozens of *L. adentus* individuals accumulated on the floodplain or in a mid-stream pond, and that the bones subsequently underwent partial disarticulation, limited hydraulic sorting via current action, and rapid burial. Evidence of currents includes the presence of small-scale ripple cross-lamination at the top of the bone-bearing interval, uneven distribution of skeletal elements (e.g., over- representation of Voorhies Group II elements), and alignment of bones within the deposit (*in situ* bone measurements provide a bidirectional vector mean of 78.1°–258.1°; Fig. 4). However, carcasses of

TABLE 4.—*MDA determination for* Lotosaurus *Quarry. Asterisk signifies that the rejection function was used in Isoplot to calculate the maximum depositional age, which resulted in the youngest grain (225.6 Ma) being rejected from the age calculation.*

		Sample	
Analysis		16-1-15-3	17-1-15-1A
YSG	Age ± 1σ	225.6 ± 2.64	248.5 ± 2.95
YPP	Age	232.6	250.8
YDZ	Age	225.67	247.67
	Range	+5.1 / -6	+4.6 / -6
	Confidence	95%	95%
WA (youngest 5)	Age	233.6 ± 8.3	253.8 ± 6.0
	Confidence	95%	95%
	Rejection	0	0
	MSWD	5.1	2.8
	Probability	0	0.025
WA (youngest 5*)	Age	236.3 ± 8.0	255.0 ± 7.0
	Confidence	95%	95%
	Rejection	0	0
	MSWD	2.7	2.4
	Probability	0.046	0.069

L. adentus likely remained partially articulated due to soft tissues that were not yet decomposed completely, and therefore articulated bone elements may not have been able to freely orient themselves in the flow, rendering the vector questionable as an indication of the paleocurrent direction (Voorhies 1969; Rogers et al. 2007).

Fractal analysis results allow for some additional inferences regarding the taphonomic agents that were active during formation of the *Lotosaurus* bonebed. In general, there is a high degree of bone grouping ($D \sim 1.6$) within the bonebed. This could reflect the fact that only limited disarticulation occurred, leaving some bones from the same individual 'grouped' together as either a tightly associated cluster or an actual articulated unit such as a partial limb or vertebral column. Weathering and strong winnowing processes can be ruled out as primary taphonomic influences on bone distribution since they would have led to bone removal, increasing spacing between elements and reducing spatial density (e.g., lowering D). Substantial transport can be ruled out since partial skeletons are discernable within the bonebed, and transport would likely have led to greater disarticulation. Axial elements appear to be the most commonly articulated bones in the quarry, and both axial and appendicular elements are likely driving the observed bone grouping ($D \sim 1.2$ for both bone types, whereas girdle elements yield $D \sim 1$). The most likely cause of this distribution is minor winnowing and currents.

There are wide variations in the length of appendicular and girdle elements in the quarry, with for instance, the largest femur (42 cm in length) measuring over twice the length of the smallest (18 cm in length). A similar level of size variation is evident in the measured axial skeletal elements (see online Supplemental File). Considered together, these data suggest that individuals of a range of different ages, likely including both adults and juveniles, are present in the assemblage.

Any plausible taphonomic scenario for the *Lotosaurus* Quarry must account for the deposition of several dozen largely but not completely disarticulated *L. adentus* skeletons in a small area, with limited evidence of weathering and no indications of damage to the bones from trampling, predation, scavenging, or insect activity. The excellent preservation of most of the bones recovered from the quarry, together with the persistence of occasional partially intact skulls, mandibles, limb elements and vertebral columns, implies that transport was minimal and that the animals died as part of a mass-mortality event. However, the event was probably not

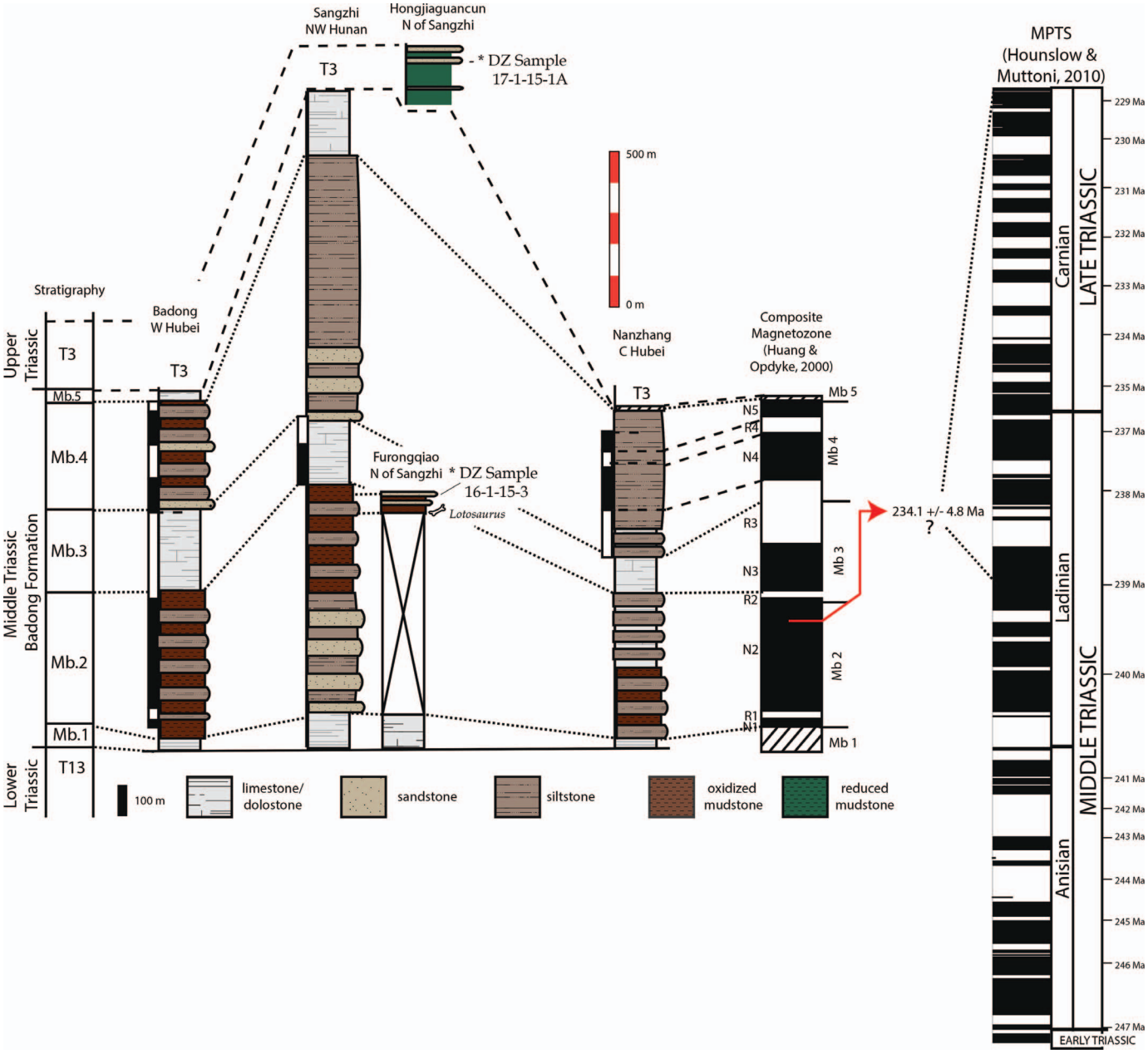

FIG. 9.—Correlation of the *Lotosaurus* Quarry section at Furongqiao and the Upper Triassic section at Hongjiaguancun to the measured sections and magnetostratigraphy of the Badong Formation established by Huang and Opdyke (2000). Maximum depositional ages from this study for the *Lotosaurus* Quarry section are used to recalibrate the magnetostratigraphy of Huang and Opdyke (2000) using the updated Magnetic Polarity Time Scale of Hounslow and Muttoni (2010). Figure is modified from both Huang and Opdyke (2000) and Hounslow and Muttoni (2010).

violent or catastrophic, such as a flood or landslide, as these typically produce death assemblages mostly comprising articulated carcasses. The limited weathering and lack of damage to the bones from insects or carnivorous tetrapods suggest that burial followed relatively soon after the deaths of the various individuals. The dozens of *L. adentus* individuals preserved in the quarry likely died as part of a single event. Although there is insufficient evidence to confirm the cause of mortality, evidence for repeated wetting and drying cycles and a semi-arid climate points tentatively to drying up or contamination of a dwindling water source in a floodplain setting. Whatever the case, the carcasses lay exposed on the floodplain for a short period, decomposing to the point where current action, during a flood or the rainy season, could bring about disarticulation, minor winnowing of small elements and realignment of larger individual bones. Scavenging during this time may explain the presence in the quarry of the temnospondyl and archosauriform teeth noted in the 2012 excavations, although whatever scavenging activity took place appears to have left no traces on the bones. Burial occurred relatively rapidly, as a result of subsequent channel reactivation or overbank flooding.

Detrital Zircon Provenance and Paleogeographic Implications

A key question concerning *L. adentus* pertains to its paleobiogeographic origins. It is uncertain whether *L. adentus* was endemic to the SCC, or whether this taxon was native to the NCC but successfully dispersed to the

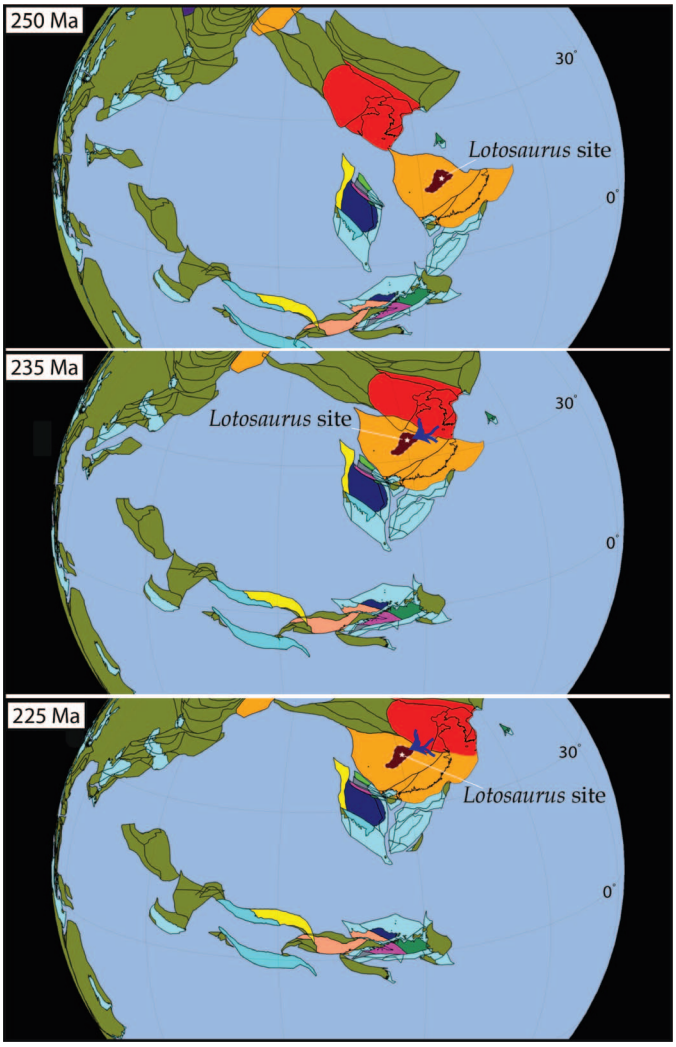

FIG. 10.—Paleogeographic reconstruction of the tectonic assembly of southeast Asia during the Late Permian to Late Triassic. Constructed via GPLATES V.16 and based on the most recent global plate reconstructions of Matthews et al. (2016) for 225 Ma, 235 Ma, and 250 Ma. Location of the *Lotosaurus* Quarry is indicated on the SCC at each time interval.

SCC as a result of terrestrial connectivity between the two cratons. Figure 10 shows the known outcrop distribution of the Badong Formation on the SCC, as well as the positions of the SCC and NCC as modeled using GPLATES V.16 (after Matthews et al. 2016) at three different times: 250 Ma, 235 Ma, and 225 Ma. During the Early Triassic and early Middle Triassic, much of the SCC was covered by a shallow marine carbonate platform succession (Yangtze Platform; Enos et al. 2006 and references therein). The Badong Formation represents a generally shallowing upward succession, characterized by deep water turbidites to the west and shallower platform carbonates and tidal flat clastics to the east (Enos et al. 2006). However, we demonstrate that for at least part of the deposition of member 2 fully continental conditions existed in northern Hunan Province (e.g., in the Sangzhi area), and fully alluvial facies have also been documented near the top of member 2 in central Hubei Province (Liu 2016). These observations suggest that collision of the two blocks had already occurred by the time the member 2 strata in question were being deposited, and that faunal interchange was possible. Furthermore, the refined MDA presented above indicates that the bonebed is younger than previously thought (~ 234–236 Ma), making post-collision deposition even more likely. In an effort to test this hypothesis in an effective manner, we have utilized a combination of paleocurrent analysis, detrital zircon geochronology, and zircon Lu-Hf isotope analysis to determine whether sediments from the *Lotosaurus* Quarry can be conclusively linked to either the NCC or the SCC. Linkage to the NCC would imply fluvial drainage from the NCC into the SCC, and hence terrestrial connectivity between the cratons.

Paleocurrent Analysis.—Paleocurrent directions were measured on three-dimensionally preserved trough cross-bedding or flute casts in channel, sheet splay, crevasse channel, and crevasse splay deposits, at multiple horizons in member 2 of the Badong Formation. Five sandstone bodies throughout the *Lotosaurus* Quarry yielded a total of 33 paleocurrent measurements, which show consistent southwesterly paleoflow regardless of facies, suggesting a northeastern source (Fig. 2). It is interesting to note that both channel facies and floodplain facies yielded consistent flow directions, which may indicate a relatively steep depositional slope at this time.

Detrital Zircon Provenance.—A brief discussion of the proposed sources of zircon populations identified in this study is provided below, and a more detailed provenance analysis for each population is given in the online Supplemental File. The first thing that stands out is the wide distribution, but low abundance, of Archean to Mesoproterozoic grain ages (Fig. 7). In general, the wide range of different zircon populations, particularly from the Badong Formation, is more consistent with sources along the southern margin of the NCC and QD regions than with sources in the SCC (Chen and Fu 1992; Chen and Zhao 1997; Zheng et al. 2006; Yokoyama et al. 2007; He et al. 2009; Yu et al. 2009; Zhu et al. 2011; Yan et al. 2011; Zhao and Cawood 2012; Ni et al. 2014). Although possible sources do exist on the SCC, they would imply much further transport distances in most cases (Zeng and Yan 2014). Neoproterozoic zircon populations in both samples have equally plausible sources in the QD and SCC (e.g., Weislogel et al. 2010; Wang et al. 2013; Nance et al. 2014; Su et al. 2014; Zhou et al. 2016). However, early Paleozoic zircon populations in both samples match best with known QD sources (Zhou et al. 2004, 2016; Yan et al. 2011; Dong et al. 2011). Similarly, late Paleozoic and early Mesozoic zircon populations closely match the ages of granitic plutons in the QD belt (Zhou et al. 2016) and throughout the Songpan-Ganzi complex (Weislogel et al. 2010). Zhang et al. (2015) also concluded that sediments deposited in the northern part of the SCC during the Triassic were most likely derived from the southern part of the QD belt.

Detrital Zircon Lu-Hf Analysis.—A small subset of grains (n = 17) was assessed via Lu-Hf isotope analysis, which was conducted primarily to test whether the Hf model ages for the main detrital zircon populations matched patterns observed by Metcalfe et al. (2013). Metcalfe et al. (2013; Fig. 8B) compiled zircon Hf model ages for the Tarim Block, NCC, and SCC, and their results suggested fairly discrete differences in zircon age distribution among these three regions could be detected in previously published data. Their compilation indicates a strong peak in the distribution between 2.9–1.9 Ga for the NCC (n = 2600 grains), and a distinctly different peak between ~ 3.7–3.3 Ga for the SCC (n = 62). The Tarim Block showed peaks at 2.6 and 3.2 Ga (n = 102).

Our 17 Lu-Hf ages indicate that most of the key detrital zircon populations can be traced back to recycled crustal sources with strongly negative εHf(t) ratios (Fig. 8A). Calculation of zircon Hf model ages for these grains reveals a wide spectrum of mostly Proterozoic model ages, which are more broadly consistent with model ages compiled by Metcalfe (2013) for the NCC. However, the wide variability in εHf(t) ratios and model ages is consistent with a broad range of sources, as might be

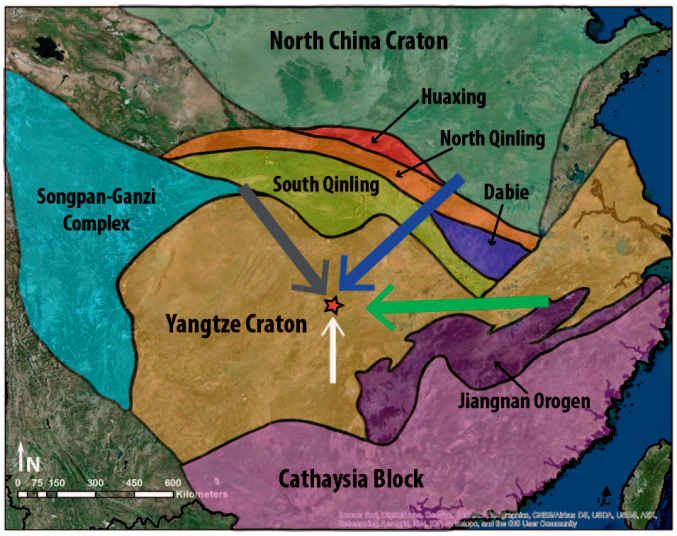

FIG. 11.—Map showing possible source terranes for zircon grains, constructed in ArcGIS 10.2.1. Three possible paleodrainage routes are shown in blue, gray, and green. An unlikely fourth route (north-directed flow from the SCC) is shown in white. Based on likely zircon provenances and regional paleocurrent data, we consider the blue route most probable. (Geologic regions adapted from Li et al. 2015 and Mao et al. 2014).

expected for zircons from an area near an active orogenic belt (e.g., the QD belt).

Implications of Zircon Provenance

During the Late Triassic, the northwestern regions of the SCC witnessed a transition from deposition of shallow marine carbonates to that of terrestrial sediments as a result of collision between the SCC and the NCC (Chen et al. 1994). New paleocurrent and detrital zircon data reported herein agree with paleodrainage reconstructions by Dong et al. (2013) and suggest that many of the zircon populations in this sample are likely sourced from the QD belt or the southern margin of the NCC, indicating the existence of a connection between the two cratons (Fig. 11). Additional support for connection prior to deposition of the *L. adentus* bonebed is the presence of numerous magmatic arc-derived terranes in the nearby QD belt with ages of ~ 240 Ma, which likely formed as a result of NCC–SCC collision. Virtually all the zircon grains analyzed in this study have magmatic origins, given their high Th/U ratios and concentric zonations (Corfu et al. 2003), and this is consistent with a QD belt provenance for those zircons that are ~ 240 Ma in age. Similarly, the strongly negative εHf values and broad range of Proterozoic-dominated zircon Hf model ages for each main detrital zircon population suggest a broad range of recycled crustal sources for the sediment of the Badong Formation. Although not unequivocal, the Lu-Hf data do quite strongly support a NCC and QD belt provenance due to the potential of these regions to provide the broad range of recycled crust seen in the zircon sample.

Proposed zircon provenance and paleocurrents indicate that fluvial drainage most likely flowed southwest from the border between the NCC and SCC during the Middle to Late Triassic (Fig. 11). The observed variety in age and geographic provenance of the zircons in our samples suggests that the *Lotosaurus* Quarry and surrounding area was a depocenter for the greater region. Three general routes are possible, based on inferred paleocurrents and patterns of zircon provenance. First, zircons could have been sourced primarily from the QD belt, the Jiangnan Orogen, and the SCC via a river flowing roughly east to west (shown in green in Fig. 11). Second, zircons could have been sourced primarily from the QD belt, the Songpan-Ganzi Complex, and the northern SCC via a river flowing roughly southeast (shown in gray on Fig. 11). Third, zircons could have been sourced from the southern margin of the NCC, the QD belt, and the northern SCC via a river flowing southwest (shown in blue on Fig. 11).

The first proposed route is possible but passes through a relatively small number of terranes, reducing the likelihood of sourcing zircons with a variety of ages (as seen in the frequency distribution plot). The second proposed route likewise does not pass through many terranes and requires flow opposite of all measured paleocurrents. The third proposed route is the most parsimonious given the varied zircon ages observed in our samples, passing through numerous regions known to hold many terranes with a variety of ages. Furthermore, the third route posits flow in the direction implied by known regional paleocurrent data (Weislogel et al. 2006). However, only limited data are available on the ages of different plutons south of the *Lotosaurus* Quarry, making it difficult to entirely rule out north-directed transport from the South China Craton (shown in white on Fig. 11).

Biogeographic Origins of Lotosaurus adentus

The known geographic distribution of *L. adentus* is restricted to the SCC, even assuming that the disarticulated *L. adentus*-like elements that occur occasionally at Maopingchang in Hubei (Liu and Wang 2005) and at various sites in Hunan do indeed pertain to this species. Paleocurrent and detrital zircon results from this study indicate that a continental connection between the SCC and NCC was present by the time the *Lotosaurus* Quarry was deposited, raising the possibility that *L. adentus* might have evolved on the NCC and migrated to the SCC after the two cratons became geographically continuous. However, there is no direct evidence to favor this scenario over the alternative possibility that *L. adentus* was indigenous to the SCC. Because the possible *L. adentus* specimens that occur at Maopingchang are found, like those at the *Lotosaurus* Quarry, in member 2 of the Badong Formation (Liu 2016), they offer no evidence that *L. adentus* existed on the SCC prior to the collision.

However, phylogenetic considerations offer potential insights into the biogeographic origins of *L. adentus*. Nesbitt (2011) found *L. adentus* to be nested within a clade of derived poposauroids whose other known members, including *Poposaurus*, *Sillosuchus*, *Effigia*, and *Shuvosaurus*, were all from the Upper Triassic of North or South America. Throughout the Triassic, the NCC likely had at least an intermittent terrestrial connection to North America via what is now Europe and Siberia, whereas the SCC lacked any direct connection to the rest of Laurasia except eventually through the NCC (Matthews et al. 2016). If *L. adentus* is indeed nested within an otherwise North and South American clade, then this taxon presumably reached the NCC via dispersal through Europe and Siberia, finally moving to the SCC at a time following the collision between the cratons. However, Liu and Sullivan (2017) tentatively identified an incomplete bone from the Anisian–Ladinian of Shanxi Province in northern China as a partial *Poposaurus*-like ilium, providing intriguing albeit limited fossil evidence for the presence of a non-shuvosaurid member of the derived poposauroid clade on the NCC during the Middle Triassic. This raises the possibility that derived poposauroids might have had representatives other than *L. adentus* in China at this time, but also reinforces the interpretation that the presence of *L. adentus* on the SCC most likely reflects dispersal from the NCC following the time of collision.

CONCLUSIONS

The *Lotosaurus* Quarry represents a rare continental example of a large, non-dinosaurian archosaur bonebed. Taphonomic analysis of the bonebed suggests that a single mass mortality event was responsible for the assemblage of at least 38 individuals. However, prior to final, rapid burial,

the skeletons were exposed for a short period of time, allowing for partial disarticulation, minor hydraulic sorting and alignment of bones. Sedimentologic and paleontologic data collected on-site indicate that the *Lotosaurus* Quarry was likely deposited in a seasonally wet-dry setting. The original interpretation of the paleoenvironment by Meng et al. (1995) suggested a tidal flat setting; this is unlikely given the sedimentology of the site and the now better-understood timing of collision between the NCC and SCC (Dong et al. 2013). Based on these combined results, the bonebed is best interpreted as a mass mortality event, possibly related to congregation around a seasonal waterhole.

A population of unexpectedly young detrital zircons identified in our study from the vicinity of the *Lotosaurus* Quarry suggests that *L. adentus* probably lived during the Ladinian or even the Carnian, rather than the Anisian as previously thought. Zircon provenance suggests S–SW paleodrainage with the majority of zircon grains having been sourced from the QD belt, which agrees with regional paleocurrent data (Weislogel et al. 2006). Clay mineral assemblage data are consistent with a subtropical climate at the time of deposition, with expected MAP values of 100–150 cm. This conclusion is also supported by paleolatitude ($\sim$ 34°N), which in turn is based on the MDA of the bonebed locality (236.3 $\pm$ 8.0 Ma; Metcalfe 2013). This MDA suggests that the NCC and SCC were likely connected at the time of deposition, allowing for exchange of sediment and terrestrial tetrapods. Given that this connection was in place, it is uncertain whether *L. adentus* was endemic to the SCC or a recent immigrant from the NCC, although evidence from the distribution and phylogeny of derived poposauroids favors immigration from the NCC as the more likely alternative.

ACKNOWLEDGMENTS

We acknowledge the National Natural Science Foundation of China (No: 41472017) for funding. EMR thanks James Cook University for funding, which made collaboration possible. CJH thanks Macalester College for funding via Beltmann and travel grants. XX is supported by the National Natural Science Foundation of China (Grant No. 41688103). R. Rogers, J. Thole, A. Chapman, and C. Robins are thanked for earlier reviews of this manuscript and for numerous discussions regarding data interpretation. Dr. Yi Hu and other staff from the Advanced Analytical Centre at the AAC provided invaluable assistance with LA-ICP-MS and MC-ICP-MS data collection. Alice Webster is thanked for her help with the technical illustration of *L. adentus*. Finally, we would like to thank the Editor, Associate Editor and two anonymous reviewers, whose valuable feedback led to significant improvements to the manuscript.

SUPPLEMENTAL MATERIAL

Data are available from the PALAIOS Data Archive: http://www.sepm.org/pages.aspx?pageid=332.

REFERENCES

Behrensmeyer, A.K., 1978, Taphonomic and ecologic information from bone weathering: Paleobiology, v. 4, p. 150–162.

Birkeland, P.W., 1999, Soils and Geomorphology: Oxford University Press, Oxford, 448 p.

Black, L.P., Kamo, S.L., Allen, C.M., Aleinikoff, J.N., Davis, D.W., Korsch, R.J., and Foudoulis, C., 2003, TEMORA 1: a new zircon standard for Phanerozoic U-Pb geochronology: Chemical Geology, v. 200, p. 155–170.

Brusatte, S.L., Benton, M.J., Desojo, J.B., and Langer, M.C., 2010, The higher-level phylogeny of Archosauria (Tetrapoda: Diapsida): Journal of Systematic Palaeontology, v. 8, p. 3–47.

Butler, R.J., Brusatte, S.L., Reich, M., Nesbitt, S.J., Schoch, R.R., and Hornung, J.J., 2011, The sail-backed reptile *Ctenosauriscus* from the latest Early Triassic of Germany and the timing and biogeography of the Early Archosaur Radiation: PLoS ONE, v. 6, p. 1–28.

Chen, S., Wilson, C.J.L., Luo, Z., and Deng, Q., 1994, The evolution of the Western Sichuan Foreland Basin, southwestern China: Journal of Southeast Asian Earth Sciences, v. 10, p. 159–168.

Chen, Y.J. and Fu, S.G., 1992, Gold Mineralization in West Henan: China Seismological Press, Beijing, 513 p.

Chen, Y.J. and Zhao, Y.C., 1997, Geochemical characteristics and evolution of REE in the early Precambrian sediments: evidences from the southern margin of the North China Craton: Episodes, v. 20, p. 109–116.

Corfu, F., Hanchar, J.M., Hoskin, P.W.O., and Kinny, P., 2003, Atlas of zircon textures: Reviews in Mineralogy and Geochemistry, v. 53, p. 469–500.

Dickinson, W.R. and Gehrels, G.E., 2009, Use of U–Pb ages of detrital zircons to infer maximum depositional ages of strata: a test against a Colorado Plateau Mesozoic database: Earth and Planetary Science Letters, v. 288, p. 115–125.

Dixon, J.B. and Weed, S.B., 1989, Minerals in Soil Environments: Soil Science Society of America, Madison, 1244 p.

Dong, S., Gao, R., Guo, T., Zhang, Y., Hu, J., Li, J., Shi, W., and Li, Q., 2013, What drove continued continent-continent convergence after ocean closure? Insights from high-resolution seismic-reflection profiling across the Daba Shan in central China: Geology, v. 41, p. 671–674.

Dong, Y., Zhang, G., Neubauer, F., Liu, X., Genser, J., Hauzenberger, C., 2011, Tectonic evolution of the Qinling Orogen, China: review and synthesis: Journal of Asian Earth Sciences, v. 41, p. 213–237.

Dhuime, B., Hawkesworth, C., and Cawood, P., 2011, When Continents formed: Science 331, p. 154.

Enos, P., Lehrmann, D.J., Jianyong, W., Youyi, Y., Jiafei, X., Chaikin, D.H., Minzoni, M., Berry, A.K., and Montgomery, P., 2006, Triassic evolution of the Yangtze Platform in the Guizhou Province, People's Republic of China: Geological Association of America Special Paper 417, p. 1–107, Boulder, doi: https://dx.doi.org/10.1130/SPE417.

Fiorillo, 1988, Taphonomy of the Hazard Homestead Quarry (Ogallala Group), Hitchcock County, Nebraska: University of Wyoming Contributions to Geology, v. 26, p. 157–166.

Gates, T.A., 2005, The Late Jurassic Cleveland-Lloyd Dinosaur Quarry as a drought induced assemblage: PALAIOS, v. 20, p. 363–375.

Gehrels, G.E., 2012, Detrital Zircon U-Pb Geochronology: current methods and new opportunities, in C. Busby and A. Azor (eds.), Tectonics of Sedimentary Basins: Recent Advances: John Wiley and Sons, Chichester, p. 47–62.

Geng, Y.S., Du, L.L., and Ren, L.D., 2012, Growth and reworking of the early Precambrian continental crust in the North China Craton: constraints from zircon Hf isotopes: Gondwana Research, v. 21, p. 517–529.

Gower, D.J., 2000, Rauisuchian archosaurs (Reptilia, Diapsida): an overview: Neues Jahrbuch für Geologie und Paläontologie, v. 218, p. 447–488.

Guo, J., Peng, P., Chen, Y, Jiao, S., and Windley, B.F., 2012, UHT sapphirine granulite metamorphism at 1.93–1.92 Ga caused by gabbronorite intrusions: implications for tectonic evolution of the northern margin of the North China Craton: Precambrian Research, v. 222-223, p. 124–142.

He, Y., Zhao, G., Sun, M., and Xia, X., 2009, SHRIMP and LA-ICP-MS zircon geochronology of the Xiong'er volcanic rocks: implications for the Paleo-Mesoproterozoic evolution of the southern margin of the North China Craton: Precambrian Research, v. 168, p. 213–222.

Hilbert-Wolf, H.L., Roberts, E.M., Downie, R., Mtelela, C., Stevens, N.J., and O'Connor, P., 2017, Application of U-Pb detrital zircon geochronology to drill cuttings for age control in hydrocarbon exploration wells: a case study from the Rukwa Rift Basin, Tanzania: AAPG Bulletin, v. 101, p. 143–159.

Hillier, S., 2003, Quantitative analysis of clay and other minerals in sandstones by X-ray powder diffraction (XRPD), *in* R.H. Worden and S. Morad (eds.), CCa-2: International Association of Sedimentologists, Gent, p. 213–251.

Hounslow, M.W. and Muttoni, G., 2010, The geomagnetic polarity timescale for the Triassic: linkage to stage boundary definitions: Geological Society of London, Special Publication 334, p. 61–102.

Huang, K. and Opdyke, N.D., 1996, Paleomagnetism of Middle Triassic redbeds from Hubei and northwestern Hunan provinces, South China: Earth and Planetary Science Letters, v. 143, p. 63–79.

Huang, K. and Opdyke, N.D., 2000, Magnetostratigraphic investigations of the Middle Triassic Badong Formation in South China: Geophysical Journal International, v. 142, p. 74–82.

Jackson, S.E., Pearson, N.J., Griffin, W.L., and Belousova, E.A., 2004, The application of laser ablation-inductively coupled plasma-mass spectrometry to *in situ* U–Pb zircon geochronology: Chemical Geology, v. 211, p. 47–69.

Kemp, A.I.S., Foster, G.L., Scherstén, A., Whitehouse, M.J., Darling, J., and Storey, C., 2009, Concurrent Pb–Hf isotope analysis of zircon by laser ablation multi-collector ICP-MS, with implications for the crustal evolution of Greenland and the Himalayas: Chemical Geology, v. 261, p. 244–260. doi:10.1016/j.chemgeo.2008.06.019

Li, J., Wu, X., and Zhang, F. (eds.), 2008, The Chinese Fossil Reptiles and Their Kin, second edition: Science Press, Beijing, 473 p.

Li, Y., Xu, Z., Pei, X., Zhang, J., Zhao, J., Zhang, L., and Wu, Y., 2015, The probability of the Mianlue suture zone, South Qinling extends to Dabie-Sulu UHP belt, East Qinling: constraint from the activity time of Ningshan shear zone: Acta Petrologica Sinica, v. 12, p. 3595–3608.

Liu, J., 2016, *Yuanansuchus maopingchangensis* sp. nov., the second capitosauroid temnospondyl from the Middle Triassic Badong Formation of Yuanan, Hubei, China: PeerJ, 4:e1903, doi: 10.7717/peerj.1903.

Liu, J. and Sullivan, C., 2017, New discoveries from the *Sinokannemeyeria-Shansisuchus* Assemblage Zone: 3, Archosauriformes from Linxian, Shanxi, China: Vert Palasiat, v. 55, p. 107–125.

Liu, S.F., Steel, R., and Zhang, G.W., 2005, Mesozoic sedimentary basin development and tectonic implication, northern Yangtze Block, eastern China: record of continent-continent collision: Journal of Asian Earth Science, v. 25, p. 9–27.

Liu, J. and Wang, Y., 2005, The first complete mastodonsauroid skull from the Triassic of China: *Yuanansuchus laticeps* gen. et sp. nov.: Journal of Vertebrate Paleontology, v. 25, p. 725–728.

Long, X.P., Yuan, C., Sun, M., Zhao, G.C., Xiao, W.J., Wang, Y.J., Yang, Y.H., and Hu, A.Q., 2010, Archean crustal evolution of the northern Tarim Craton, NW China: Zircon U-Pb and Hf isotopic constraints: Precambrian Research, v. 180, p. 272–284.

Ludwig, K.R., 2012, User's Manual for Isoplot 3.75: A Geochronological Toolkit for Microsoft Excel: Berkeley Geochronology Centre, Berkeley, 75 p.

Mao, S., Chen, Y., Zhou, Z., Lu, Y., Guo, J., Qin, Y., and Yu, Y., 2014, Zircon geochronology and Hf isotope geochemistry of the granitoids in the Yangshan gold field, western Qinling, China: implications for petrogenesis, ore genesis and tectonic setting: Geological Journal, v. 49, p. 359–382.

Matthews, K.J., Maloney, K.T., Zahirovic, S., Williams, S.F, and MÜller, D., 2016, Global plate boundary evolution and kinematics since the late Paleozoic: Global and Planetary Change, v. 146, p. 226–250.

Meng, F., 1996, Floral palaeoecological environment of the Badong Formation in the Yangtze Gorges Area: Geology and Mineral Resources of South China, v. 4, p.1–13.

Meng, F., Xu, A., Zhang, Z., Lin, J., and Yao, H., 1995, Nonmarine biota and sedimentary facies of the Badong Formation in the Yangzi and its neighbouring areas: China University of Geosciences Press, Wuhan, 76 p.

Metcalfe, I., 2013, Gondwana dispersion and Asian accretion: tectonic and palaeogeographic evolution of eastern Tethys: Journal of Asian Earth Sciences, v. 66, p. 1–33.

Moore, D.M. and Reynolds, R.C., 1997, X-Ray Diffraction and the Identification and Analysis of Clay Minerals: Oxford University Press, Oxford, 400 p.

Morag, N., Avigad, D., Gerdes, A., Belousova, E., and Harlavan, Y., 2011, Crustal recycling in the northern Arabian-Nubian Shield: new perspectives from zircon Lu-Hf and U-Pb systematics: Precambrian Research, v. 186, p. 101–116.

Munroe, M.A., and Blenkinsop, T.G., 2012, MARD-a moving average rose diagram application for Geosciences: Computers and Geoscience, v. 49, p. 112–120.

Næraa, T., Scherstén, A., Rosing, M.T., Kemp, A.I.S., Hoffmann, J.E., Kokfelt, T.F., and Whitehouse, M.J., 2012, Hafnium isotope evidence for a transition in the dynamics of continental growth 3.2 Gyr ago: Nature, v. 485, p. 627, doi:10.1038/nature11140.

Nance, R.D., Murphy, J.B., and Santosh, M., 2014, The supercontinent cycle: a retrospective essay: Gondwana Research, v. 25, p. 4–29.

Nesbitt, S., 2007, The anatomy of *Effigia okeeffeae* (Archosauria, Suchia), theropod-like convergence, and the distribution of related taxa: Bulletin of the American Museum of Natural History, v. 302, p. 1–84.

Nesbitt, S., 2011, The early evolution of archosaurs: relationships and the origin of major clades: Bulletin of the American Museum of Natural History, v. 352, p. 1–292.

Nesbitt, S.J., Desojo, J.B., and Irmis, R.B., 2013, Anatomy, phylogeny and palaeobiology of early archosaurs and their kin: Geological Society London Special Publications, v. 379, p. 1–7.

Ni, Z.Y., Li, N., and Zhang, H., 2014, Hydrothermal mineralization at the Dahu Au-Mo deposit in the Xiaoqinling gold field, Qinling Orogen, central China: Geological Journal, v. 49, p. 501–514.

Parrish, J.M., 1993, Phylogeny of the Crocodylotarsi, with reference to Archosaurian and Crurotarsan Monophyly: Journal of Vertebrate Paleontology, v. 13, p. 287–308.

Rieppel, O., 1999, The sauropterygian genera *Chinchenia*, *Kwangsisauraus*, and *Sanchiaosaurus* from the Lower and Middle Triassic of China: Journal of Vertebrate Paleontology, v. 19, p. 321–337.

Rogers, R.R., Eberth, D.A., and Fiorillo, A.R., 2007, Bonebeds: Genesis, Analysis, and Paleobiological Significance: The University of Chicago Press, Chicago, 512 p.

Su, J., Dong, S., Zhang, Y., Li, Y., Chen, X., and Cui, J., 2014, Detrital zircon geochronology of pre-Cretaceous strata: tectonic implications for Jiangnan Orogen, South China: Geological Magazine, v. 151, p. 1–21.

Tang, H., Hu, X., Deng, Q., and Xiong, C., 2009, Research on the characteristics and slope deformation regularity of the Badong Formation in the Three Gorges Reservoir Area, *in* F. Wang and T. Li (eds.), Landslide Disaster Mitigation in Three Gorges Reservoir, China: Springer-Verlag, Berlin Heidelberg, p. 87–113.

Tucker, R.T., Roberts, E.M., Hu, Y., Kemp, A.I.S., and Salisbury, S.W., 2013, Detrital zircon age constraints for the Winton Formation, Queensland: contextualizing Australia's Late Cretaceous dinosaur faunas: Gondwana Research, v. 24, p. 767–779.

Tucker, R.T., Roberts, E.M., Kemp, A.A., and Henderson, B., 2016, Large igneous province or long-lived magmatic arc along the eastern margin of Australia during the Cretaceous? Insights from the sedimentary record: GSA Bulletin, v. 128, p. 1461–1480.

Van Achterbergh, E., Ryan, C.G., Jackson, S.E., and Griffin, W.L., 2001, Appendix 3, data reduction software for LA-ICP-MS, *in* P. Sylvester (ed.), Laser-Ablation-ICPMS in the Earth Sciences-Principles and Applications: Mineralogical Association of Canada, Short Course Series, p. 239–243.

Voorhies, M., 1969, Taphonomy and population dynamics of an early Pliocene vertebrate fauna, Knox County, Nebraska: University of Wyoming Contributions to Geology, Special Paper 1, 69 p.

Wang, W., Zhou, M.F., Yan, D.P., Li, L., and Malpas, J., 2013, Detrital zircon record of Neoproterozoic active-margin sedimentation in the eastern Jiangnan Orogen, South China: Precambrian Research, v. 235, p. 1–19.

Webb, J.A., 1979, A reappraisal of the palaeecology of conchostracans (Crustacea: Branchiopoda): Neues Jahrbuch für Geologie und Palaöntologie, Abhandlungen, v. 158, p. 259–275.

Weislogel, A., Graham, S., Chang, E., Wooden, J., and Gehrels, G., 2010, Detrital zircon provenance from three turbidite depocenters of the Middle-Upper Triassic Songpan-Ganzi complex, central China: record of collisional tectonics, erosional exhumation, and sediment production: GSA Bulletin, v. 122, p. 2041–2062.

Weislogel, A., Graham, S., Chang, E., Wooden, J., Gehrels, G., and Yang, H., 2006, Detrital zircon provenance of the Late Triassic Songpan-Ganzi complex: sedimentary record of collision of the North and South China blocks: Geological Society of America, v. 34, p. 97–100.

Yan, Y., Hu, X., Lin, G., Santosh, M., and Chan, L., 2011, Sedimentary provenance of the Hengyang and Mayang basins, SE China, and implications for the Mesozoic topographic change in South China Craton: evidence from detrital zircon geochronology: Journal of Asian Earth Sciences, v. 41, p. 494–503.

Yin, H., 2006, Triassic biostratigraphy of China, *in* W. Zhang, P. Chen, and A.R. Palmer (eds.), Biostratigraphy of China: Science Press, Beijing, p. 379–422.

Yokoyama, K., Tsutsumi, Y., Lee, C.S., Shen, J.J.S., Lan, C.Y., and Zhao, L., 2007, Provenance study of Tertiary sandstones from the Western Foothills and Hsuehshan Range, Taiwan: Bulletin of the National Museum of Natural Science C, v. 33, p. 7–26.

Yu, J.H., Wang, L., O'Reilly, S.Y., Griffin, W.L., Zhang, M., Li, C., and Shu, L., 2009, A Paleoproterozoic orogeny recorded in a long-lived cratonic remnant (Wuyishan terrane), eastern Cathaysia Block, China: Precambrian Research, v. 174, p. 347–363.

Zeng, L. and Yan, L.L., 2014, Petrogenesis and geochronology of Cretaceous adakitic, I- and A-type granitoids in the NE Yangtze block: constraints on the eastern subsurface boundary between the North and South China blocks: Comment: Lithos, v. 196-197, p. 376–379.

Zhang, F., 1975, A new theocodont *Lotosaurus* from Middle Triassic of Hunan: Vertebrate PalAsiatica, v. 13, p. 144–147.

Zhang, K.J., Cai, J.X., Zhang, Y.X., and Zhao, T.P., 2006, Eclogites from central Qiangtang, northern Tibet (China) and tectonic implications: Earth and Planetary Science Letters, v. 245, p. 722–729.

Zhang, Z.L. and Meng, F.S., 1987, Biostratigraphy of the Yangtze Gorge Area (4): Triassic and Jurassic: Geological Publishing House, Beijing, 408 p. [In Chinese]

Zhang, Y., Jia, D., Shen, L., Yin, H., Chen, Z., Li, H., Li, Z., and Sun, C., 2015, Provenance of detrital zircons in the Late Triassic Sichuan foreland basin: constraints on the evolution of the Qinling Orogen and Longmen Shan thrust-fold belt in central China: International Geology Review, v. 57, p. 1806–1824.

Zhang, Y.X., Zeng, L., Li, Z.W., Wang, C.S., Zhang, K.J., Yang, W.G., and Guo, T.L., 2015, Late Permian–Triassic siliciclastic provenance, palaeogeography, and crustal growth of the Songpan terrane, eastern Tibetan Plateau: evidence from U-Pb ages, trace elements, and Hf isotopes of detrital zircons: International Geology Review, v. 57, p. 159–181.

Zhao, G. and Cawood, P.A., 2012, Precambrian geology of China: Precambrian Research, v. 222–223, p. 13–54.

Zheng, Y.F., Zhao, Z.F., Wu, Y.B., Zhang, S.B., Liu, X.M., and Wu, F.Y., 2006, Zircon U–Pb age, Hf and O isotope constraints on protolith origin of ultrahigh-pressure eclogite and gneiss in the Dabie orogeny: Chemical Geology, v. 231, p. 135–158.

Zhou, C., Tucker, R., and Xiao, S., 2004, New constraints on the ages of Neoproterozoic glaciations in South China: Geology, v. 32, p. 437–440.

Zhou, Z., Mao, S., Chen, Y., and Santosh, M., 2016, U-Pb ages of Lu-Hf isotopes of detrital zircons from the southern Qinling Orogen: implications for Precambrian to Phanerozoic tectonics in central China: Gondwana Research, v. 35, p. 323–337.

Zhu, X.Y., Chen, F., Li, S.Q., Yang, Y.Z., Nie, H., Siebel, W., and Zhai, M.G., 2011, Crustal evolution of the North Qinling terrain of the Qinling Orogen, China: evidence from detrital zircon U-Pb ages and Hf isotopic composition: Gondwana Research, v. 20, p. 194–204.

Received 5 October 2017; accepted 4 February 2018.